Sommario

Abstract 3

Riassunto 5

Introduction 7

Chapter 1. Geological Setting 9

1.1 Geographical Setting 9

1.2 Geological Setting of the Dent Blanche Tectonic System 10

1.3 Introduction to the Petrography of the Valpelline and Arolla Series 12

1.3.1 The Arolla Series 12

1.3.2 The Valpelline Series 12

1.4 Pre-Alpine Metamorphism of the Valpelline Series 13

1.5 Alpine Metamorphism of the Valpelline Series 15

Chapter 2. Fieldwork Activity 17

Chapter 3. Fluid and Melt Inclusions 29

3.1 Fluid Inclusions 29

3.2 Silicate Melt Inclusions 35

3.3 Nanogranitoids 37

3.3.1 Analytical Techniques to Investigate Nanogranitoids 39

Chapter 4. Analytical and Experimental Methodologies 41

Chapter 5. Petrography and Microstructures 47

5.1 Petrography 47

5.1.1 Valp6 47

5.1.2 Valp8b 53

5.1.3 Valp11 58

5.2 Nanogranitoid Inclusions 63

5.2.1 Remelting Experiments and Chemistry of the Melt 67

5.3 Chemical Analysis of the Host Garnet 71

Chapter 6. Discussion 73

6.1 Host Rocks 73

6.2 Microstructures of Inclusions and Re-melting Experiments 74

Chapter 7. Conclusions 77

Ringraziamenti.....79
References.....81
Appendix.....87

Abstract

Since their discovery melt inclusions (MI) have been a very useful tool in igneous petrology and from the last decade they represent a novel approach for the study of metamorphic rocks.

This work focuses on the investigation of high-grade metapelitic rocks (*kinzigites*) from the Valpelline Series and on the characterization of the melt inclusions hosted in peritectic garnet. These rocks belong to the Australpine domain of the western Alps and represent portions of the southern continental margin of the alpine Tethys. The partial melting in this rocks occurred at about 750-850 °C and 6-8 kbar during the Permian (300-250 Ma).

One hundred and one samples have been collected from the Valpelline Series and seventy-seven thin sections have been prepared from them. Subsequently a preliminary work with the optical microscope has been done in order to identify the most promising samples for the study of MI. A detailed microstructural characterization has been performed on selected samples using electron scanning microscope (SEM-EDS). The inclusions are small in size (< 20 μm) and are of primary origin as testified by their distribution in the cores of peritectic garnet. They are formed by a polycrystalline assemblage of quartz + plagioclase + K-feldspar + biotite and they are call *nanogranites or nanogranitoids;* no glassy inclusions have been founded in any samples.

An important goal of this work was the re-homogenization of MI in order to recover the bulk composition of the trapped melt. This has been done via remelting experiments under confining pressure in a piston cylinder apparatus.

The inclusions did not re-homogenize after the first experiment conducted at 800 °C and 10 kbar for 24 hours and, hence, it was necessary to perform a second experiment at 850 °C and 10 kbar for 24 hours. In this case almost all nanogranite inclusions were partially re-melted but some of them displayed interaction with the host garnet, such as the recrystallization of garnet around the inclusions or the

crystallization of new phases (e.g., orthopyroxene) at the inclusion wall. This occurs because the trapping temperature of MI was exceeded during the experimental run. One inclusion was almost totally re-homogenized, without clear evidence of overheating. Semi-quantitative analyses have been done using EDAX system.

For the first time the probable composition of the melt produced by the partial melting of crustal rocks of the Valpelline Series was analysed ($SiO_2 \approx 72\%$, $Na_2O \approx 2\%$, $CaO \approx 0.7\%$, $K_2O \approx 6\%$, $FeO \approx 4\%$, $Al_2O_3 \approx 13\ \%$).This work also confirms the previous temperature estimates from the literature on peak conditions of the Variscan metamorphism.

Riassunto

Fin dalla loro scoperta le inclusioni di fuso silicatico (*melt inclusions*, MI) sono state uno strumento fondamentale utilizzato per problematiche di petrologia ignea. A partire dall'ultimo decennio, esse rappresentano anche un nuovo approccio per lo studio delle rocce metamorfiche di alta temperatura come migmatiti e granuliti.

Questo lavoro di tesi si focalizza sullo studio di rocce metapelitiche di alto grado metamorfico (*kinzigiti*) della Serie di Valpelline e sulla caratterizzazione delle inclusioni di fuso silicatico situate all'interno di granati peritettici. Queste migmatiti appartengono al dominio Australpino delle Alpi Occidentali e rappresentano porzioni del margine continentale meridionale della Tetide Alpina. La fusione parziale di queste rocce è avvenuta circa a 750-850 °C e 6-8 kbar durante il Permiano (300-250 Ma).

Durante il lavoro di terreno effettuato nella Valpelline (Valle d'Aosta) sono stati raccolti centouno campioni dai quali sono state preparate settantasette sezioni sottili. Successivamente, per identificare i campioni più promettenti per lo studio delle MI, è stato svolto un lavoro preliminare su tutte le sezioni sottili attraverso l'utilizzo del microscopio ottico. Sui campioni selezionati è stata poi eseguita una caratterizzazione microstrutturale di dettaglio utilizzando un microscopio a scansione elettronica (SEM-EDS). Le inclusioni rinvenute nei granati peritettici sono di piccole dimensioni (< 20 μm) e sono di origine primaria come testimoniato dalla loro distribuzione nei nuclei del minerale ospite. Esse sono formate da un aggregato policristallino di quarzo + plagioclasio + K-feldspato + biotite e possono essere definite *nanograniti* o *nanogranitoidi*. In nessun campione sono state trovate inclusioni contenenti del vetro preservato.

Un importante obiettivo di questo lavoro è stata la ri-omogeneizzazione delle MI al fine di recuperare la composizione originale del fuso intrappolato. Questo è stato effettuato grazie ad esperimenti a pressione di confinamento controllata utilizzando il piston cylinder.

Dopo il primo esperimento condotto a 800 °C e 10 kbar per 24 ore, le inclusioni non si sono ri-omogeneizzate del tutto, ma sono risultate solo parzialmente rifuse. È stato, quindi, necessario effettuare un secondo esperimento a 850°C e 10 kbar per 24 ore. In questo caso le inclusioni di nanogranitoidi tendono a mostrare evidenze di interazione con il granato ospite, come la ricristallizzazione del granato attorno alle inclusioni o la formazione di nuove fasi (ad esempio, ortopirosseno) nel bordo interno delle inclusioni. Questi risultati indicano che la temperatura di intrappolamento delle MI è stata superata durante il secondo esperimento. Le fasi all'interno delle inclusioni dopo gli esperimenti di rifusione sono state caratterizzate utilizzando il sistema SEM-EDAX. Una sola inclusione si presenta quasi totalmente ri-omogenizzata, senza evidenze di sovra-riscaldamento.

Attraverso l'analisi dell'inclusione ri-omogenizzata, per la prima volta è stata analizzata la probabile composizione del fuso anatettico prodotto dalla fusione parziale delle rocce crostali della Serie di Valpelline. Esso presenta una composizione granitica ($SiO_2 \approx 72\%$, $Na_2O \approx 2\%$, $CaO \approx 0.7\%$, $K_2O \approx 6\%$, $FeO \approx 4\%$, $Al_2O_3 \approx 13\%$). Questo lavoro conferma anche le precedenti stime di temperatura del picco metamorfico Varisico proposte dalla letteratura.

Introduction

Melt inclusions (MI) are small droplets of melt (appearing now from glassy to crystallized) entrapped within host minerals during their growth. MI have been extensively used in igneous petrology, igneous geochemistry and volcanology to obtain chemical and physical information on magmatic systems and processes (Lowenstern 1995; Frezzotti 2001).

In the last ten years melt inclusions have become an important tool even in metamorphic petrology for the study of partially-melted high grade terranes (migmatites and granulites). In this case melt inclusions are trapped during incongruent reactions by the growing peritectic host (Cesare et al. 2009). The first case study was that of glassy inclusions hosted in peritectic garnet and plagioclase from partially melted metapelite enclaves of El Hoyazo dacite, SE Spain (Cesare 1997) (Acosta-Vigil et al. 2010, 2007). In these rocks the melt inclusions were quenched by the fast cooling of the host dacite and they now appear as glassy MI.

After this first finding, partially to totally crystallized melt inclusions were subsequently found in common high grade metamorphic terranes. The slow cooling permitted the crystallization of different phases from the trapped melt as documented in the migmatitic granulites from the Kerala Khondalite Belt, Southern India (Cesare et al. 2009; Ferrero et al. 2012). This type of melt inclusions containing a cryptocrystalline aggregate of quartz, feldspars and micas were called *nanogranites* (Cesare et al. 2009) and then *nanogranitoids* (Cesare et al. 2015).

The studies of nanogranites may provide important advantages to the characterization of partially melted terrains, because their composition represents the composition of the primary anatectic melt produced in the early stages of crustal melting. Conversely, the composition of leucosomes and S-type granites is not representative of that of primary melts because of differentiation processes such as fractional crystallization, cumulus phenomena and entrainment of peritectic minerals (Brown 1994; Marchildon and Brown 2001; Sawyer 2008).

Migmatitic rocks of the Valpelline Series (Australpine domain, Western Alps, Italy) have been selected for this study of melt inclusions because, with respect to the analogous Ivrea-Verbano zone from the Southern Alps where nanogranites have been investigated (Carvalho et al. 2018), here melt inclusions have never been documented.

The research started with a field work to collect migmatitic rocks along the Valpelline Valley. Then all the rocks have been studied from the petrographic view point to identify samples containing workable melt inclusions. On the selected samples, a detailed microstructural study has been performed to characterize the melt inclusions using electron scanning microscope (SEM) and, subsequently, two re-melting experiments were carried out using a piston cylinder apparatus. Inclusions are not completely re-homogenized after the first experiments at 800 °C. Instead, after the second run at 850 °C, some MI are almost totally re-homogenized but there is evidence of interaction between the host garnet and inclusions (overheating of inclusions).

The presence of *nanogranites* has been confirmed for the first time in the Valpelline Series and the probable composition of the melt produced by the partial melting of these rocks during the Variscan metamorphism has been obtained.

Chapter 1. Geological Setting

The Alps are a double-vergent orogen, developed since the Cretaceous as a result of the convergence between Europe and Adria, which is considered a promontory of the Africa plate (Manzotti et al. 2012).

In the Western Alps, the compression involved both continental units from Adriatic and European margins, and oceanic slices derived from the Mesozoic Piemonte-Liguria ocean (Handy et al. 2010; Dal Piaz 2001). The continental units, derived from the Adriatic margin, are referred to as the Australpine Domain and they show evidence of Variscan and post-Variscan metamorphism (see below).

1.1 Geographical Setting

The Regione Autonoma Valle d'Aosta, Italy, is located into the Pennine and Graie Alps, between Piedmont, France and Switzerland.

The area of my study is located along the Valpelline valley in the Italian Western Alps (fig. 1.1) at about 14 km N-E of Aosta. This sector of the western Alps is included between the Penninic frontal thrust (PF) to the north, and the Aosta - Ranzola (AR) and Ospizio Sottile (OS) fault systems to the south. The Simplon normal fault (SF) and the Canavese tectonic line (CL) close respectively this sector to the north-northeast and to the east.

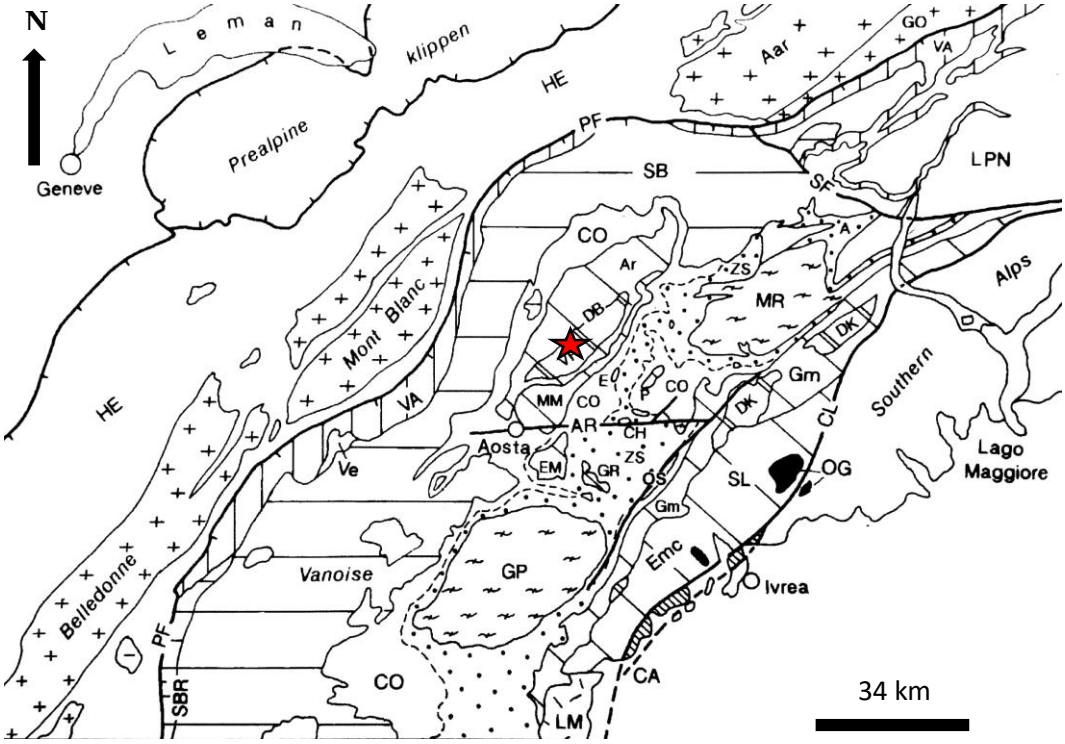

fig. 1.1. Tectonic map of Western Alps, taken from" Carta geologica della Valle d'Aosta 1.100000", and modified from Dal Piaz, 1999. The red star indicates the area of sampling.

1.2 Geological Setting of the Dent Blanche Tectonic System

The area of my study is comprised in the Dent Blanch Tectonic System (DBTS) (Manzotti et al. 2014) (fig. 1.2). The DBTS, is thought to have been coherent with the Sesia-Lanzo zone located to the SE (fig. 1.1), because of lithological and geochronological similarities (Gardien et al. 1994; Compagnoni et al. 1977). The DBTS consists of two main basement nappes: 1) the Dent Blanche s.s. nappe (to the northwest), which embraces two main units defined as the structurally lower Arolla Series and the Valpelline Series at higher structural levels; 2) the Mont Mary nappe (to the southeast), which includes two different lithological units, named as Upper-Mont Mary and Lower-Mont Mary. The two nappes are separated by the Roisan-Cignana Shear Zone (RCSZ).

The Sesia-Lanzo zone consists of a polycyclic meta-sedimentary basement intruded by granitoid and gabbroic bodies (Compagnoni et al. 1977) showing Carboniferous

and Permian ages of metamorphism. It has been divided into three units: 1) the Gneiss Minuti Complex; 2) the II Zona Dioritico-Kinzigitica (II DK); 3) the Eclogitic Micaschists Complex. The dominant metamorphism in this nappe developed under blueschist and eclogitic facies conditions, with the formation of abundant lawsonite.

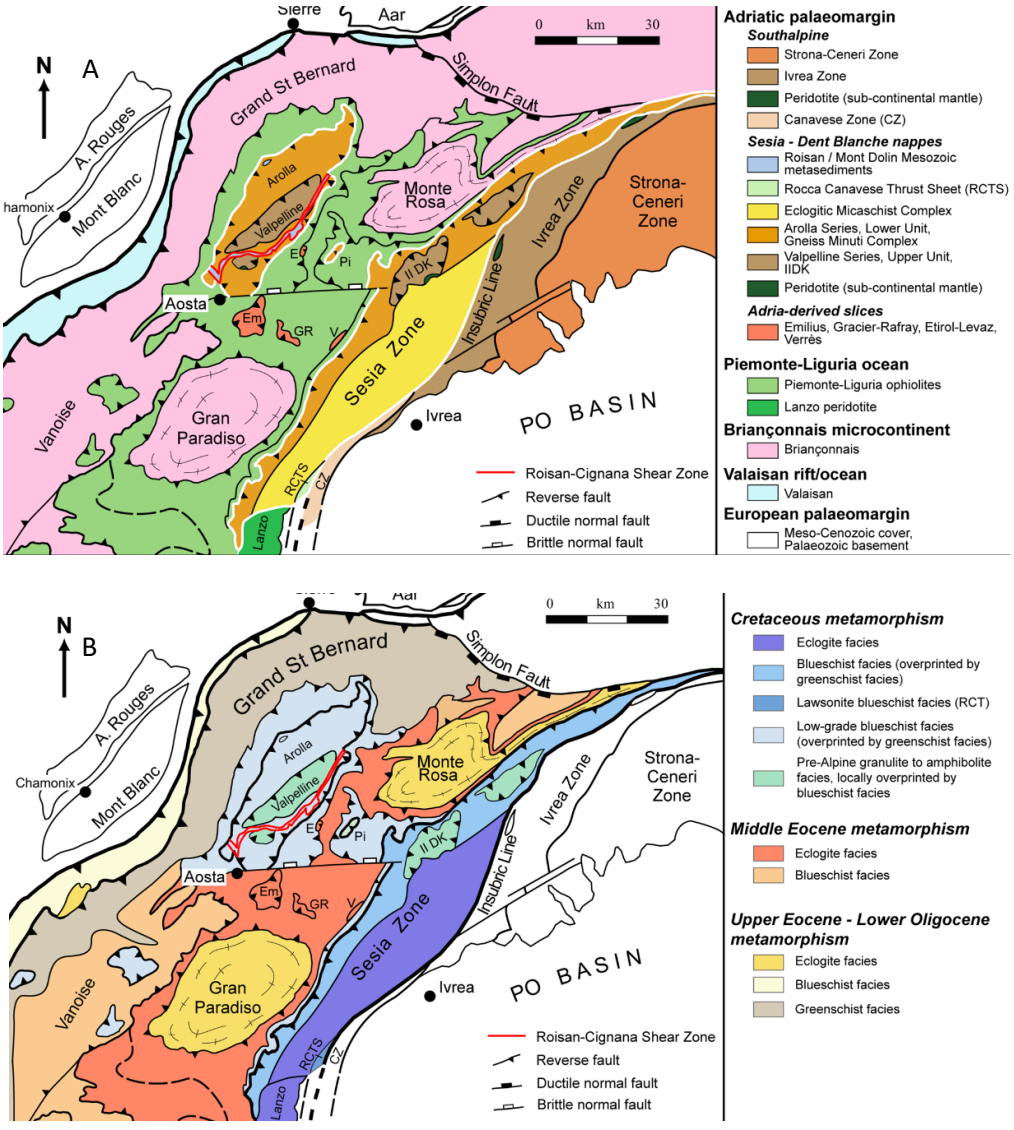

fig. 1.2. (A) Simplified tectonic map of the north-western part of the Western Alps. (B) metamorphic map of the same area where the age and the grade of the Alpine metamorphism are combined (Manzotti et al. 2014; LeBayon and Ballèvre 2006).

1.3 Introduction to the Petrography of the Valpelline and Arolla Series

The Arolla Series of the DBTS is composed by Permian age rocks (granites, clinopyroxene-bearing granites, diorites, gabbros) which have been metamorphosed and deformed during the Alpine tectonometamorphic events into gneisses, orthogneisses and schists (De Leo et al. 1987; Pennacchioni and Guermani 1993; Zucali and Roda 2008).

The Valpelline Series is composed by pre-Alpine high-grade paragneisses with lenses and layers of marbles, mafic granulites and clinopyroxene-bearing amphibolites (Manzotti and Zucali 2013).

1.3.1 The Arolla Series

The major part of massive rocks of the Arolla Series is represented by meta-granites. They consist of quartz, plagioclase, biotite, amphibole, subhedral alkali feldspar, white mica, epidote, ilmenite and chlorite (Diehl et al. 1952; Manzotti 2011). Gneisses represent the most important rock-type of the Arolla Unit. In particular, it is possible to recognize orthogneisses containing quartz, phengite, plagioclase, a sodic- and calcic-amphibole, epidote, ilmenite, chlorite and gneisses characterized by quartz, feldspar, hornblende, garnet, epidote, phengite, chlorite and titanite (Manzotti 2011). There are also quartzodiorites composed by plagioclase + quartz + biotite + euhedral hornblende (as magmatic assemblage) + white mica + epidote + ilmenite (as metamorphic mineral assemblage) (Manzotti 2011; Diehl et al. 1952).

1.3.2 The Valpelline Series

The Valpelline Series consists of high grade rocks metamorphsed under upper-amphibolites facies to granulites facies conditions. The common lithotype is

represented by para-gneisses with garnet, biotite and sillimanite, commonly named *"kinzigites"* (Compagnoni et al. 1977). These rocks show a migmatitic structure where the melanosome consists of garnet + biotite ± sillimanite and the leucosome of quartz + plagioclase + K-feldspar. In addiction there are garnet-pyroxene-bearing amphibolites that contain plagioclase, hornblende, diopside, ilmenite and locally garnet. Interlayered with kinzigites and amphibolites are olivine ± phlogopite-bearing marbles containing calcite + dolomite and minor olivine ± phlogopite ± pyroxene ± garnet, amphibole, white mica and ilmenite (Manzotti 2011).

1.4 Pre-Alpine Metamorphism of the Valpelline Series

The pre-Alpine metamorphic history of the Valpelline Series of the Dent Blanche nappe s.s. can be divided into four stages (fig. 1.3). The conditions of the first stage (S1, about 290-300 Ma) are 700-800 °C and 9-10 kbar (Gardien et al. 1994). The temperature values were determined by biotite-garnet geothermometer of Ferry and Spear (1978) on garnet core composition and included biotite. The pressure values were determined by the garnet-plagioclase-Al-silicate-quartz geobarometer of Ghent (1976) on garnet core composition and included plagioclase (Gardien et al. 1994). Phase S1 is marked by the reaction:

muscovite + quartz = K-feldspar + Al-silicate + liquid.

The second stage (S2) corresponds to the peak T in pre-Alpine evolution. This is marked by the reaction:

biotite + quartz + Al-silicate + plagioclase = K-feldspar + garnet + liquid

at about 750-850°C and 6-8 kbar (Manzotti et al. 2014). Permian ages (290-260 Ma) were found for S2 based on U-Pb geochronology and it is related to the Permo-Triassic thinning (Manzotti et al. 2012, 2014; Zucali and Spalla 2011).

The third stage (S3) is characterized by a decrease in temperature, testified by the destabilization of the alkali feldspar-garnet assemblage into biotite-sillimanite.

Cordierite is locally present; conditions of 3.5-4.5 kbar and 650-700°C were proposed for the appearance of this mineral (Gardien et al. 1994).

During the fourth stage (S4) temperature decreased down to greenschist facies conditions. While alkali feldspar and cordierite broke down into white mica, chlorite formed at the rims of biotite and garnet indicating a temperature of 500°C and a pressure of 3-4 kbar testified by the pseudomorphs of kyanite after sillimanite (Gardien et al. 1994; Pennacchioni and Guermani 1993).

In conclusion, the Valpelline Series (with Upper Unit of Mont Mary nappe and II DK) represents a slice of late-Palaeozoic anatectic lower crust (Compagnoni et al. 1977) and this is supported by three reasons: (1) these units consist of high-temperature rocks equilibrated at typical deep-crustal conditions; (2) they display a great quantity of partial melting features and (3) they lack granitoid intrusions, which are typical of upper crustal conditions (Manzotti et al. 2014).

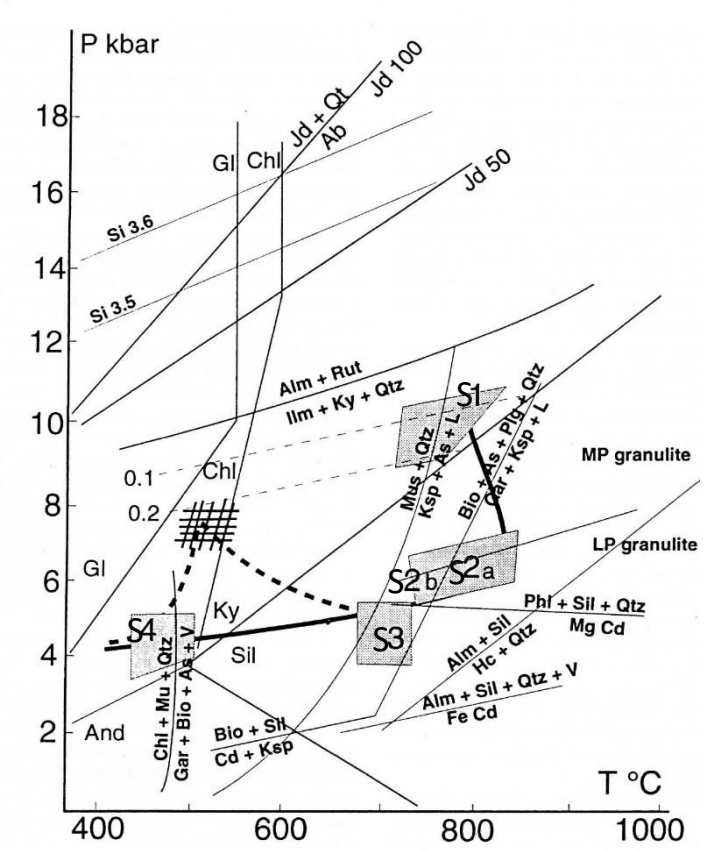

fig. 1.3. Pre-Alpine P-T path of the paragneisses of the Valpelline Series. (Gardien et al. 1994).

1.5 Alpine Metamorphism of the Valpelline Series

The Alpine metamorphism in the DBTS comprises a Eoalpine and a Mesoalpine phase. The former (Late Cretaceous, 100-90 Ma) is characterized by HP-LT conditions that are typical of subduction environments. The latter is related to the exhumation processes and is characterized by the development of greenschist facies mineral assemblages (fig. 1.4).

In the DBTS, the Alpine metamorphism did not overprint homogeneously the pre-Alpine associations of the two tectonic units. While it was pervasive in the Arolla unit, in the Valpelline unit the blueschist facies conditions are not reached and we can only see a greenshist facies overprinting of the older higher-grade assemblages.

The Arolla Series (Lower Element of the Dent Blanche nappe) is coherent with the Eclogitic Micaschist Complex and Gneiss Minuti (Gardien 1994) but the HP-LT conditions reached by rocks of these units are different. In the Arolla Series a lower pressure condition has been reached, testified by the preservation of the igneous plagioclase in metagranitoids without development of jadeitic pyroxene. In the Eclogitic Micaschist Complex, on the contrary, the plagioclase of the igneous protholiths is totally transformed into jadeite + quartz + zoisite. This suggests that in the Arolla Series the Eoalpine metamorphism reached lower pressures (in the blueschist facies) than in the Eclogitic Micaschist Complex (eclogite facies) (Compagnoni et al. 1977; Manzotti et al. 2014; Dal Piaz 1971).

The Mesoalpine phase occurred during Late Eocene-Early Oligocene age (41-28 Ma) and is characterized by the exhumation to shallower structural levels of the subduction complex, which was overprinted by a Barrovian-type metamorphism Dal Piaz e al. 2003). During this phase superimposed strain patterns are documented in the Dent Blanche s.s. (Pennacchioni and Guermani 1993; Manzotti et al. 2014). This strain intensity varies, from one unit to the next and in the same unit. In particular, the Valpelline Series preserves extensively the pre-Alpine structures and mineral assemblages. Probably this occurred because rocks were strongly dehydrated during the pre-Alpine metamorphism and therefore they did not react

under retrograde HP-LT conditions of the Eoalpine phase. Usually a pervasive Alpine strain and mineral assemblages can be found in narrow shear zones (Manzotti et al. 2014).

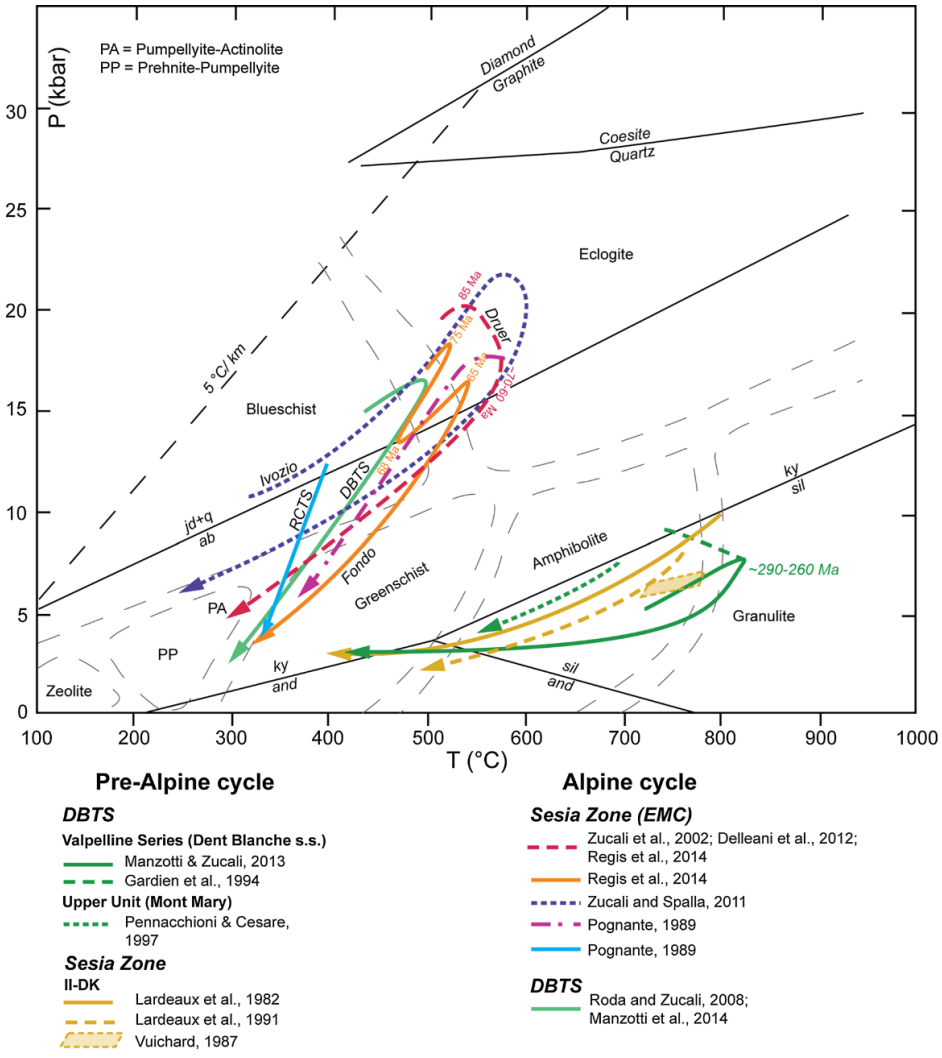

fig. 1.4. Pre-Alpine and alpine P-T paths for the Dent Blanche Tectonic System and the Sesia Zone (Manzotti et al. 2014).

Chapter 2. Fieldwork Activity

The first phase of this work was focused on sampling of anatectic rocks along the Valpelline valley, Valle d'Aosta (fig. 2.1). I spent nine days in the field during two periods; the first one at the end of July and the second during the last week of August, 2017. All the GPS coordinates, the elevation and the labels of the collected samples are reported in tab. 2.1 (at the end of this chapter).

fig. 2.1. Waypoint (WPT) projection of sampling sites in Valpelline valley.

Rocks that are described below are migmatites and for their macroscopic characterization I will refer to Sawyer (2008).

Migmatite is a medium- and high-grade metamorphic rock that partially melted and that consists of two or more different parts: the two principal are paleosome and neosome. Paleosome is defined as part of migmatite that was not affected by partial melting where structures older than the partial melting are preserved. Neosome is the part of migmatite newly formed by partial melting. It contains a fraction derived from the crystallization of the melt and another fraction that consists of the minerals

that are remained solid: either the products of incongruent melting reactions or the minerals that were refractory or in excess in the reaction that produced the melt. Melanosome and leucosome are the terms that must be used to refer to the parts of neosome. Melanosome is the darker-colored part of the neosome and it is the solid residual fraction left after part of the melt fraction has been segregated. It is dark coloured because is formed by Fe- and Mg-bearing minerals such as biotite, garnet, and orthopyroxene. Leucosome is the lighter-colored part of the neosome consisting of plagioclase, quartz and K-feldspar. It derives from the crystallization of the segregated partial melt (Sawyer 2008).

One hundred and one samples were collected during the field activity (tab. 2.1). Here I describe the most important outcrops. The first one is located behind the Chalet Prarayer, on the footpath which leads to the Chalet Aosta (WPT 008 in fig. 2.1). The rock is a dilation-structured metatexite migmatite (fig. 2.2). A metatexite is heterogeneous migmatite at outcrop scale and showing pre-anatectic structures preserved in the paleosome and in the melanosome (Sawyer 2008). An evident foliation is visible which probably predates the formation of the migmatite. The mineral assemblage is composed of garnet + biotite + K-feldspar + plagioclase + quartz and, therefore, the protholith is likely to be an aluminous metapelite.

In the same area a decametric scale leucocratic zone can be observed. The presence of some radial injection veins developed in the surrounding migmatite together with the high amount of leucocratic material could suggest it is a zone of accumulation of the anatectic melt produced in the area (fig. 2.3).

In the same area I observed dykes crosscutting the foliation of the migmatites and the small leucosome developed along the foliation (fig. 2.4). These leucocratic bodies could reflect the injection of granitic melts coming from other source rocks.

fig. 2.2. Metatexite migmatite. Garnet is present in small crystal everywhere in the rock, both in leucosome and melanosome. Red lines indicate the pre-melting foliation. Under the coin it is possible to observe the leucosome that is located in dilatant structural sites.

fig. 2.3. Zone of melt accumulation. Above the coin one can see the presence of some injection veins.

fig. 2 4. Example of granitic dyke which crosscuts the foliation of the migmatites.

The second important outcrop is located along the road that connect Dzovennoz to Bionaz where a diatexite migmatite is exposed (WPT 001 in fig. 2.1). A diatexite is a migmatite where neosome is dominant and melt was pervasively distributed throughout. In a diatexite pre-partial-melting structures are not visible in the neosome (Sawyer 2008). The melanosome shows very small garnet and biotite grains. The leucosome contains large garnet, plagioclase, quartz and K-feldspar crystals (fig. 2.5).

A great peculiarity of this outcrop is the presence of large “double colour” garnets (fig. 2.6). At hand-specimen scale a dark nucleus and a pink rim are often visible.

Continuing on the same road towards south-west (WPT 011 in fig. 2.1), there is a stromatic or layer-structured metatexite migmatite (fig. 2.7 and fig. 2.8). The melanosome contains biotite and garnet. The leucosome consists of plagioclase, K-feldspar and quartz.

fig. 2.5. Diatexite migmatite. The coin is in the melanosome. On the right one can see a large quantity of granitic melt and garnet crystal of peritectic origin.

fig. 2.6. Garnet with the pink rim and dark black core.

fig. 2.7. Metatexite migmatite with stromatic structure.

fig. 2.8. The finger indicates a cm-scale boudin, formed by plagioclase, K-feldspar and quartz (same outcrop as in fig. 2.7).

The third important outcrop is located at Oyace, near the Chiesa Parrocchiale di Oyace (WPT 006 in fig. 2.1). Here there is a dilation-structured metatexite migmatite. The melanosome shows small and pink garnet without apparent alteration (fig. 2.9).

In the same outcrop there are two boudins. These structures usually form where single competent layers are extended into separate pieces through plastic, brittle or a combination of plastic and brittle deformation mechanisms (Fossen 2016) (fig. 2.10).

There is also a pegmatitic vein crossing the right part of the outcrop, and filled with quartz + K-feldspar + plagioclase (fig. 2.11).

fig. 2.9. Metatexite migmatite. The melanosome shows abundant pink garnets.

fig. 2.10. Two boudins of dark colour surrounded by plastically deformed matrix.

fig. 2.11. Leucocratic vein contains grey quartz and euhedral feldspars.

The last important outcrop for this work is located at an amphibolite quarry (WPT 007 in fig. 2.1) where I collected the sample Valp11 containing the polycrystalline inclusions investigated in this study (see below). It is a diatexite migmatite formed at upper-amphibolite-facies metamorphic conditions. The melanosome is formed by garnet + biotite. The leucosome is composed by quartz + K-feldspar + plagioclase + garnet (fig. 2.12). There was not sillimanite or other aluminous polymorphs.

fig. 2. 12. (A) Melanosome assemblage of clinopyroxene + biotite surrounded by the leucosome assemblage of quartz + K-feldspar + garnet + plagioclase. (B) The yellow arrow indicates a large garnet into the leucosome.

Waypoint	*Latitude*	*Longitude*	*Elevation*	*Samples Name*
WPT1	45,870004	7,415867038	1634,68	
WPT2	45,86999796	7,415885981	1635,02	
WPT3	45,86999402	7,415890004	1635,05	
WPT4	45,89982497	7,490648031	1976,88	
WPT5	45,85034399	7,381744981	1389,85	Valp1/Valp2
WPT6	45,83361003	7,363065993	1074,44	Valp3/Valp4/Valp5/Valp6/Valp7/Valp8
WPT7	45,92560703	7,545290999	2017,95	Valp9/Valp10/Valp11/Valp12
WPT8	45,86996896	7,415808029	1587,89	Valp13/Valp14
WPT9	45,86974399	7,414776972	1589,47	Valp15/Valp16/Valp17/Valp18/Valp19
WPT10	45,86965003	7,414443959	1592,59	Valp20/Valp21
WPT11	45,869501	7,414075993	1594,50	Valp22/Valp23/Valp24
WPT12	45,86880304	7,412397014	1594,64	Valp25/Valp26
WPT13	45,850359	7,381576002	1266,04	Valp27/Valp28
WPT14	45,86997902	7,415838037	1584,62	Valp29/Valp30/Valp31/Valp32
WPT15	45,869644	7,414347986	1584,12	Valp33/Valp34/Valp35
WPT16	45,86953	7,414032994	1584,48	Valp36/Valp37/Valp38
WPT17	45,86875702	7,412373964	1581,39	Valp39
WPT18	45,83148404	7,340629986	1219,77	Valp40/Valp41/Valp42
WPT19	45,83160197	7,340638032	1220,52	Valp43/Valp44/Valp45
WPT20	45,83162301	7,340568965	1219,47	Valp46/Valp47
WPT21	45,83173801	7,340510041	1221,85	Valp48/Valp49
WPT22	45,831994	7,34070098	1231,43	Valp50
WPT23	45,83118003	7,340558991	1142,94	Valp51
WPT24	45,831233	7,343324013	1177,77	Valp52/Valp53
WPT25	45,83117098	7,343546972	1137,59	Valp54/Valp55/Valp56

WPT26	45,83106101	7,34344597	1132,10	Valp57
WPT27	45,83059799	7,342856973	1125,70	Valp58/Valp59
WPT28	45,84945501	7,381856963	1423,01	
WPT29	45,84931201	7,382240016	1390,06	Valp60
WPT30	45,84792699	7,380340006	1301,74	Valp61
WPT31	45,84841699	7,380434973	1306,14	Valp62
WPT32	45,84907003	7,381870961	1333,33	Valp63
WPT33	45,89692902	7,488463959	1751,45	Valp64/Valp65
WPT34	45,897171	7,48829498	1776,77	Valp66/Valp67
WPT35	45,89657396	7,486692024	1784,42	Valp68
WPT36	45,89664102	7,48517096	1787,69	Valp69/Valp70
WPT37	45,89651202	7,48448398	1789,38	Valp71/Valp72/Valp73
WPT38	45,89603702	7,483315961	1790,21	Valp74
WPT39	45,89704402	7,477599001	1783,11	Valp75/Valp76/Valp77
WPT40	45,92000398	7,52043304	2179,60	Valp78
WPT41	45,92884697	7,514548022	2251,87	Valp79/Valp80
WPT42	45,89992203	7,491910011	2029,03	Valp81/Valp82
WPT43	45,90304898	7,490583993	2260,39	Valp83/Valp84/Valp85
WPT44	45,918756	7,48451801	2883,98	Valp86
WPT45	45,91466596	7,488891017	2750,82	Valp87/Valp88/Valp89/Valp90/ Valp91/Valp92/Valp93/Valp94/Valp95
WPT46	45,850389	7,381658	1584	Valp96/Valp97/Valp98/Valp99/ Valp100/Valp101

tab. 2.1. All the GPS waypoints, longitude, latitude, elevation and the labels of the samples collected in the field. Longitude and latitude refer to WGS84 system.

Chapter 3. Fluid and Melt Inclusions

The term “fluid inclusion” indicates inclusions in mineral hosts which trapped a phase that was a fluid at the temperature and pressure of formation, regardless of the present state of inclusion at ambient conditions. Trapped fluid can be liquid, vapour or supercritical fluid and its composition can be pure water, a COH fluid, brines of various salinity, gas or gas-bearing liquids and silicate, sulfide or carbonate melts (Bodnar 2003). Some terms such as “crystallized inclusion” are related to the presence of other phases than liquid or vapour at room temperature, but they are fluid inclusions by the previous definition.

3.1 Fluid Inclusions

Fluids inclusions (FI) are important in petrological studies because they can provide information which is impossible to retrieve otherwise. They can give the chemical composition of the trapped fluid and its molar volume. If the chemical composition of the fluid is in equilibrium with the mineral assemblage, the molar volume gives us the possible values of P-T conditions at which the equilibrium has been reached by means of an *isochore* (Touret 2001).

FI can have different shapes, from irregular, ovoidal, tubular to ideal “negative crystal”, following the symmetry of the host mineral (Frezzotti 2001). The colour of FI is not diagnostic, because depending on differences in refractive index and shape we can observe bright or dark inclusions with a transmitted light microscope.

At room temperature conditions FI usually are not homogeneous, but some different phases can be found within the fluid. For example, often there is a gas bubble or vapour phase within an aqueous inclusion. This second phase is simply recognizable because of its dark colour and spherical shape (fig. 3.1).

FI can trap phases that are immiscible. For example, the coexistence of silicate melt with a sulphide melt inclusion which can concentrate Ni and Cu from the silicate melt (Roedder 1984).

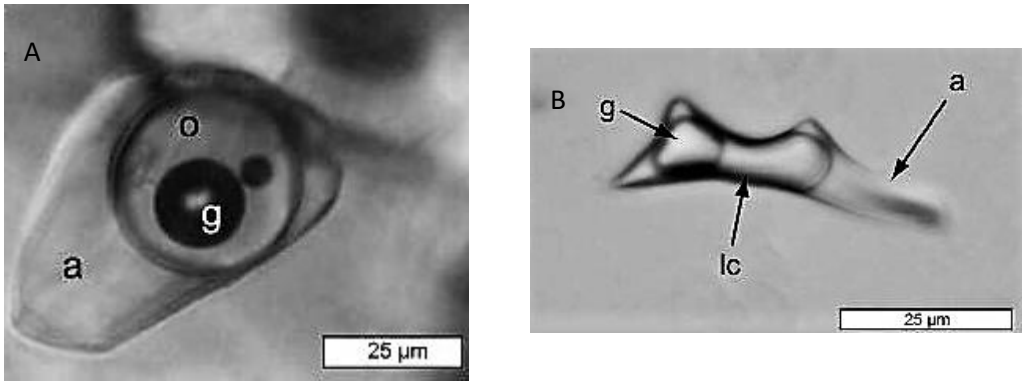

fig. 3.1. Figure A is transmitted light photomicrograph of a fluid inclusion containing 3 fluid phases: aqueous liquid (a), liquid oil (o), and gas bubble (g). Figure B is a synthetic three-phase fluid inclusion in quartz: aqueous liquid (a), liquid carbon dioxide (lc) and gas (g). (Goldstein 2003).

Fluid inclusions are divided in three types on the base of to their origins: 1) *primary*, 2) *secondary*, 3) *pseudosecondary* (fig. 3.2).

1) *primary* inclusions: this term is referred to inclusions entrapped directly during, and as a direct consewuence of, crystal growth. This type of inclusions can be easily recognized considering their microstructural position within the host mineral. For example, if inclusions are elongated in the growth direction of the host mineral or they show a zonal arrangement or are present as isolated clusters, they can be classified as primary inclusions (Roedder 1984; Goldstein 2003).
2) *secondary* inclusions: inclusions are trapped after the growth of host mineral is completed. This happens when the host has been broken by fractures and it re-crystallized, trapping droplets of the surrounding fluid. These secondary inclusions are identifiable when they appear as trails/planes. There is the possibility that two or more trails of inclusions cross each other, and if so, we can define the temporal succession thanks of them (fig. 3.3).

3) *pseudosecondary* inclusions: they are inclusions which are entrapped before mineral growth is completed, but not necessarily as a direct result of it. We find them in microfractures like secondary inclusions, but pseudosecondary inclusion differ to secondary ones because their entrapment is followed by further crystal growth. When pseudosecondary fluid inclusions are studied, they are treated like secondary ones.

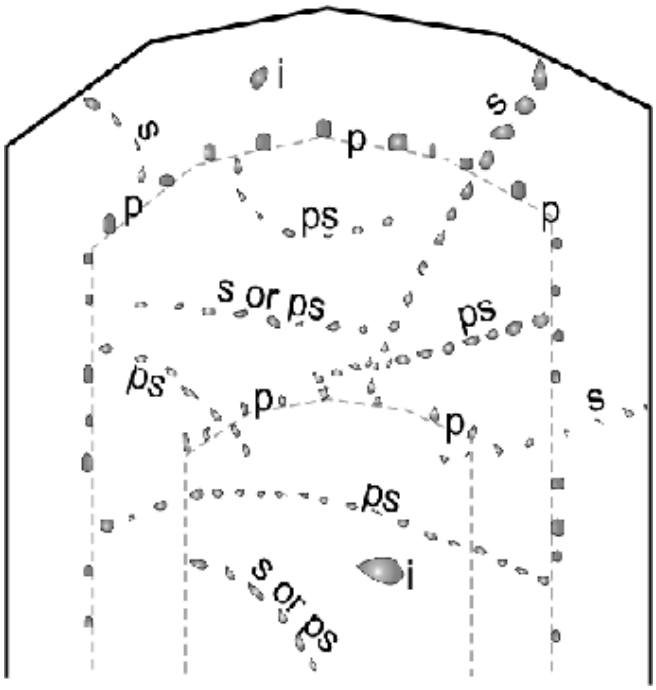

fig. 3.2. This is a hypothetical view within a single crystal showing primary (p), secondary (s), pseudosecondary (ps) and inclusions of indeterminable origin (i) (Goldstein 2003) .

Solid phases are often associated with fluid inclusion and they can be of two types: trapped or daughter inclusions. The former occur for the incorporation of a pre-existing solid phase by growth surface of a host mineral with a fluid inclusion forming at the same time.

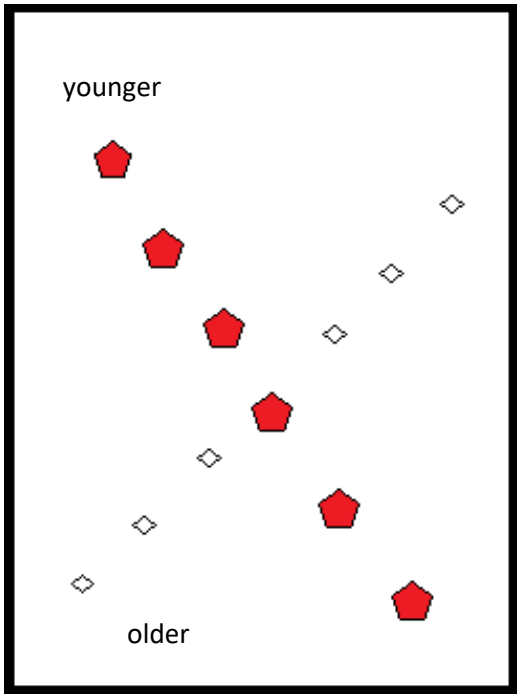

fig. 3.3. Intersection of two trails of fluid inclusions: red pentagons are younger than white rhombs.

The latter are precipitated from the inclusion fluid itself, by cooling after entrapment. These two types of solid inclusions are often distinguished by microstructures and with a microscope-mounted heating stage: the daughter solid which has precipitated from an FI during cooling, typically re-melt with increasing temperature up to the temperature of homogenization.

After the entrapment of inclusions within host minerals, some changes can occur, in particular regarding phase assemblage and physical structure. For what concerns differences in phase assemblage, there are a lot of possibilities and one of them is the host crystallization on the wall. Indeed, the trapped fluid could contain a certain percentage of the host composition, which could cause the oversaturation of the trapped fluid and, therefore, the re-crystallization of the host mineral at the edges of the inclusion.

The most important physical changes regard the shape and the volume of inclusions. The first consists of a process called necking down (fig. 3.4, 3.5, 3.6). This

transformation occurs when trapped inclusions have large surface areas, hence necking down or necking off starts to reduce the high surface energy of the system. The final result is the formation of different inclusions that have the same total volume as the parent (single) inclusion but a smaller total energy.

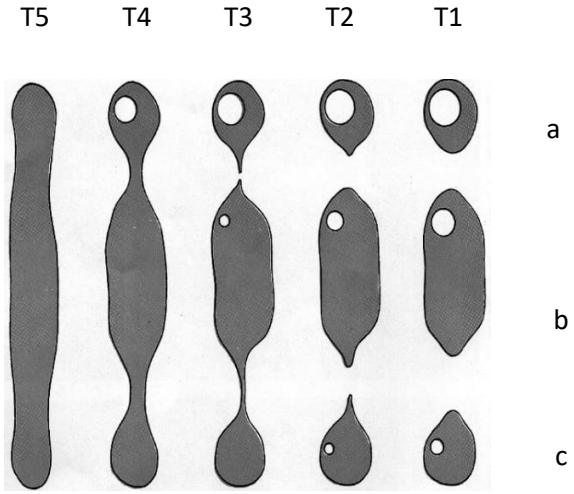

fig. 3.4. Necking down of a tubular inclusion. The original one was trapped at T5 and breaks up during slow cooling to form three different inclusions. When we make some experiments the inclusions a, b and c re-homogenized respectively at T5, between T4 and T3, between T3 and T2 (Roedder 1984).

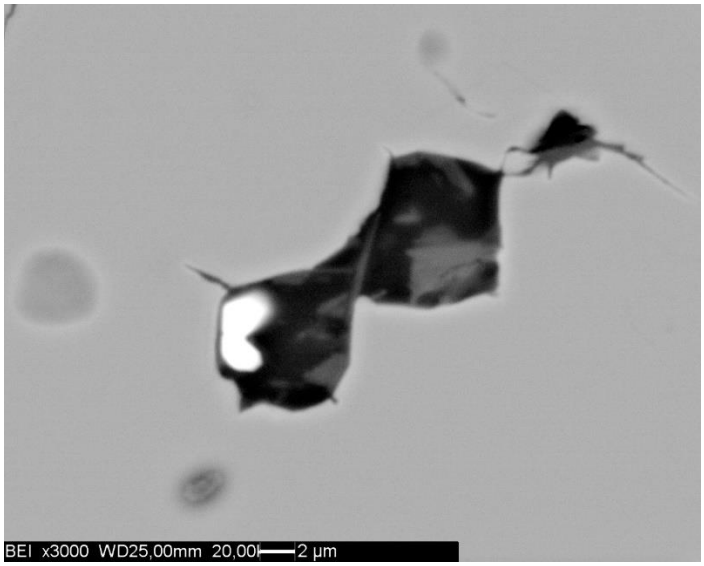

fig. 3.5. Example of necking down in melt inclusion which is not completed from sample Valp12_bis.

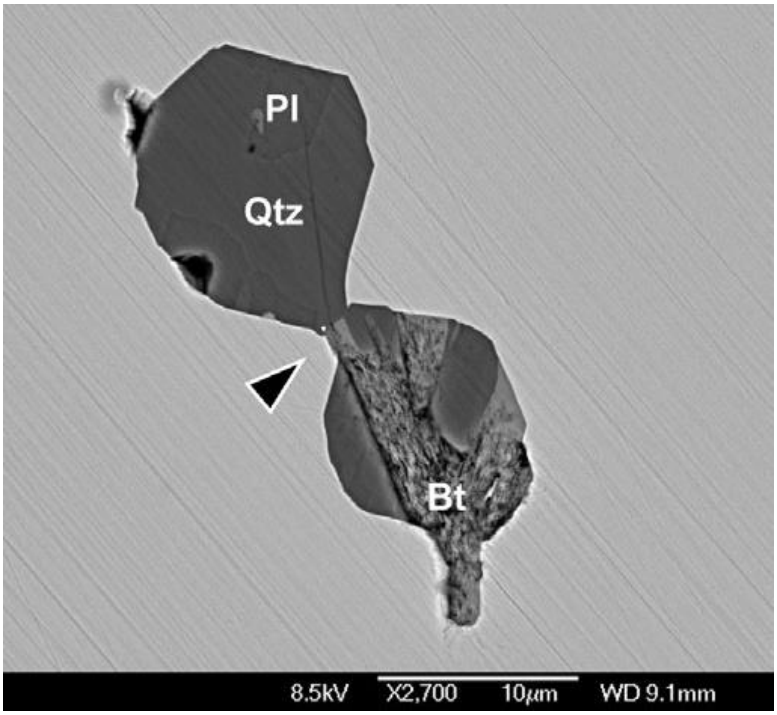

fig. 3.6. Hourglass MI underwent a partial necking down in the Barun Gneiss. The black arrow indicates the development of the neck that precede the complete separation (Ferrero et al. 2012).

The necking down process does not involve changes in composition of the inclusions, unless a fluid exsolves or a daughter phase crystallizes before the separation. In that case the composition of the two inclusions separated by the necking process will not be the same.

Volume change, can be reversible and irreversible. Reversible changes generally consist of variations that do not lead to permanent conditions. There are different mechanisms that can cause changes in fluid inclusions: (a) crystallization on the walls or on in the fluid itself (daughter minerals or daughter crystals), which have no effects on volume, if these new minerals re-melt during heating; (b) thermal contraction of the host mineral on cooling and (c) dilation changes from internal and external pressures that have two different effects (c1, c2). If there is a dilation of entire crystal causes by release of the confining pressure, there is the possibility of an enlargement of inclusion cavities within the crystal (c1); the other (c2) effect is the dilation of the host mineral immediately surrounding the inclusions as a result of the local internal pressure during homogenization run (Roedder 1984).

Irreversible changes causing permanent variations in volume. The most common example is the fracturing of the host mineral with the subsequent increase of FI volume through crack opening.

3.2 Silicate Melt Inclusions

Melt inclusions (MI), the main subject of this study, are “small droplets of silicate melt entrapped in different minerals during their growth in the presence of a melt phase” (Cesare et al. 2015; Frezzotti 2001).

Melt inclusions can be trapped via two processes: 1) incongruent melting reaction or (2) melt cooling in a magmatic environment (fig. 3.7).

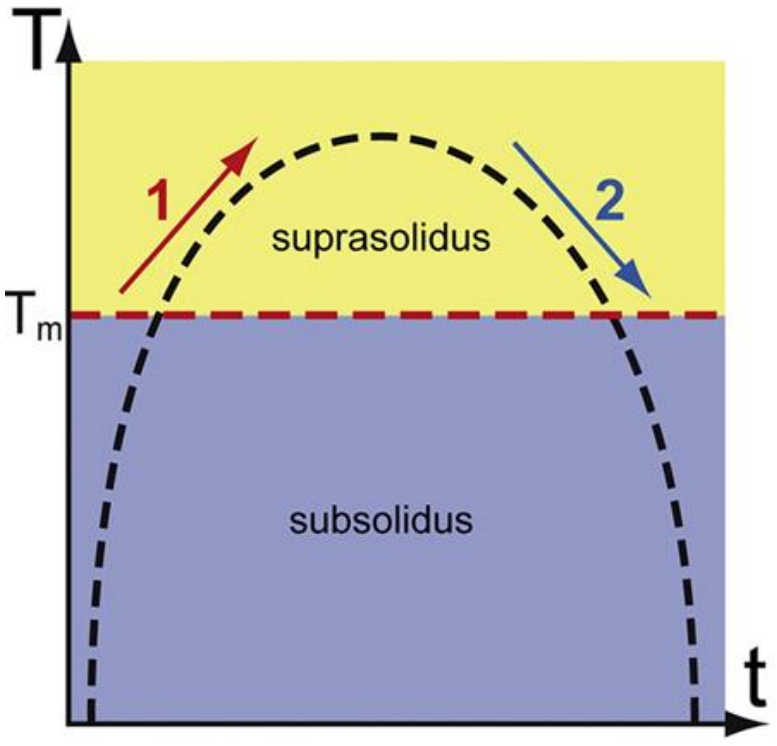

fig. 3.7. Schematic T-t diagram from Cesare et al. (2015), representing the difference between MI entrapment during peritectic melting (red arrow) and igneous crystallization (blue arrow). In the first case the host phase growth in solid framework and MI, having primary composition, are trapped during heating. In an igneous system the host mineral crystallizes from a cooling magma and droplets of evolved melt may be trapped.

Concerning the second, the host phase grows from a magma during cooling and, therefore, the composition of the trapped melt inclusions reflects that of an evolved magma. This is the main difference from the MI entrapment during incongruent melting, where MI are trapped during heating and have a primary composition reflecting the one of the peritectic melt.

A common process to have incongruent melting is crustal anatexis, which, along melt extraction, constitutes the most important mechanism of geochemical differentiation of the continental crust (Acosta-Vigil et al., 2010). A theoretical incongruent reaction can be: A + B = C + M, where A, B, C are the solids and M is the liquid phase. The phase C (peritectic mineral) is contemporary to M and has the potential to entrap primary inclusions of the coexisting liquid phse.

Melt inclusions can undergo several changes after the entrapment as the necking down process described in subchapter 3.1. Irreversible changes are important for this study because pressure differences between the inclusion and the host can cause the loss of volatiles. If pressure differences exceed the strength of the host mineral, the inclusion will explode in the case of fluid overpressure or implode for fluid under-pressure (fig. 3.8). The inclusions which are involved in such process are called “transposed” or “decrepitated” inclusions (Touret 2001).

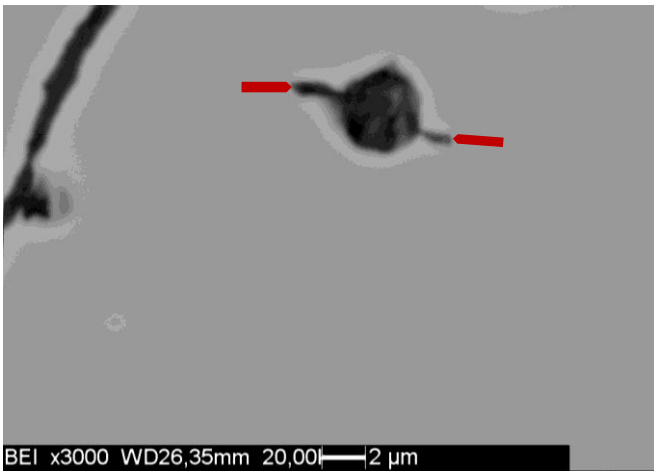

fig. 3.8. Inclusion from sample Valp8b characterized by offshoots typical of decrepitated inclusions. Red arrows indicate the two offshoots.

3.3 Nanogranitoids

Melt inclusions present different degrees of crystallization, from glassy to fully crystallized (fig. 3.9). The latter are called *nanogranitoids* after Cesare et al. (2015) (fig. 3.10). Their size ranges from a few up to a few tens of micrometres and their shape varies from irregular to negative crystal (Cesare et al. 2015). This "perfect" form is the final result of a dissolution-reprecipitation process that affects MI after their entrapment, without volume changes (Roedder 1984). The negative crystal shape is characteristic of each host mineral because it is affected by the crystal structure of the host. For example, a dodecahedron is expected in MI trapped in garnet (fig. 3.11).

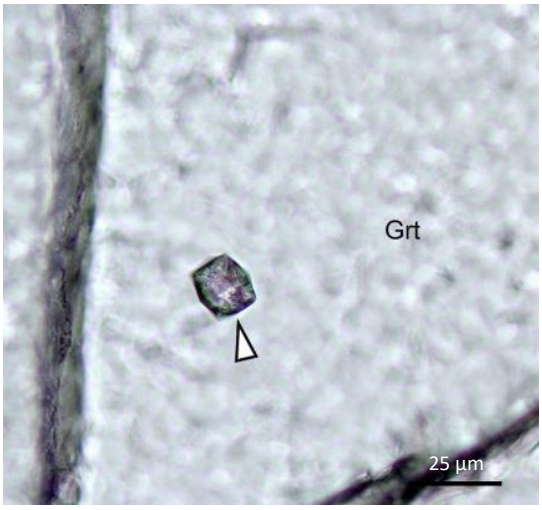

fig. 3.9. Photomicrograph of a negative crystal shape of nanogranite inclusion in garnet. Modified from Cesare et al. (2015).

Melt inclusions appear brownish at optical observation hence often we do not distinguish between glassy or crystallized inclusions. Under crossed-polarized investigations *nanogranitoids* show multiple birefringent phases while glassy inclusions show an isotropic and homogeneous phase.

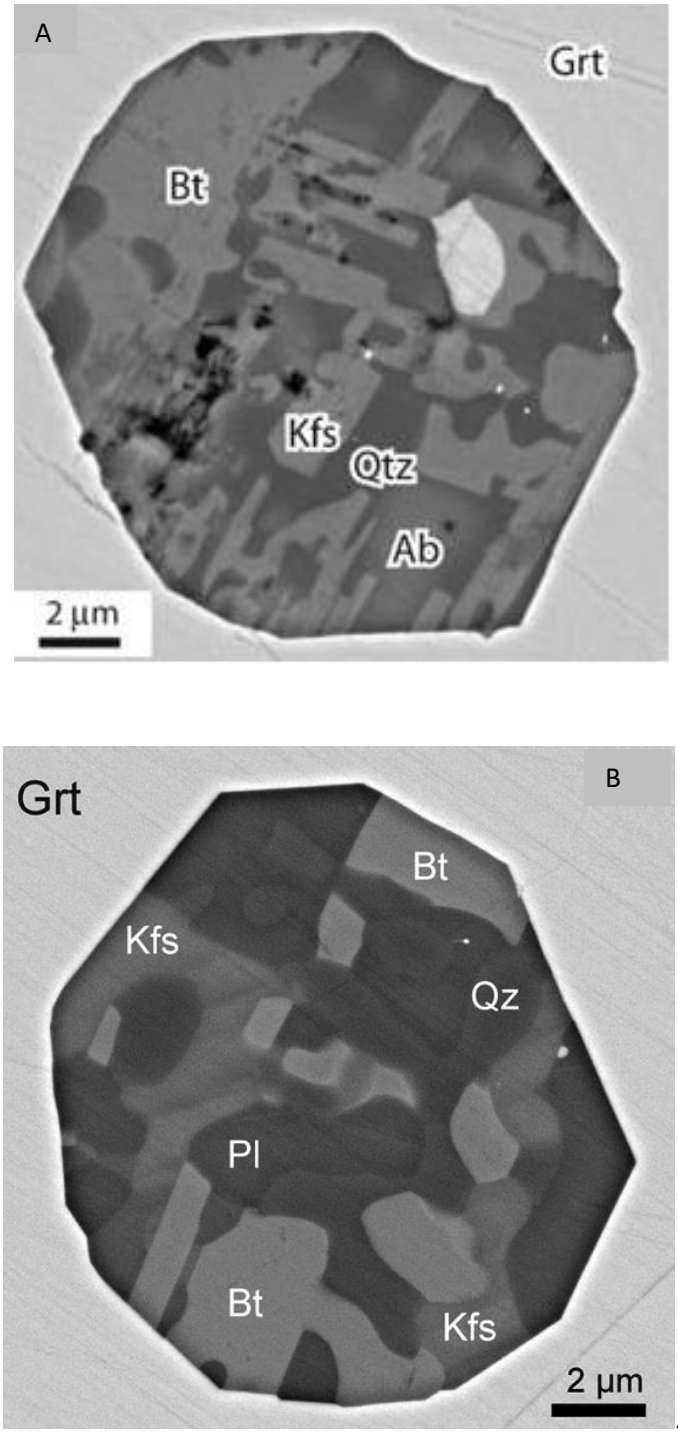

fig. 3.10. (A) Nanogranite inclusion with large crystals of biotite (Bt) and K-feldspar (Kfs) in a micrographic association with interstitial quartz (Qtz) and subordinate albite (Ab) (Cesare 2009). (B) Nanogranite inclusion in a metapelitic granulite from Kerala Khondalite Belt (Cesare et al. 2015).

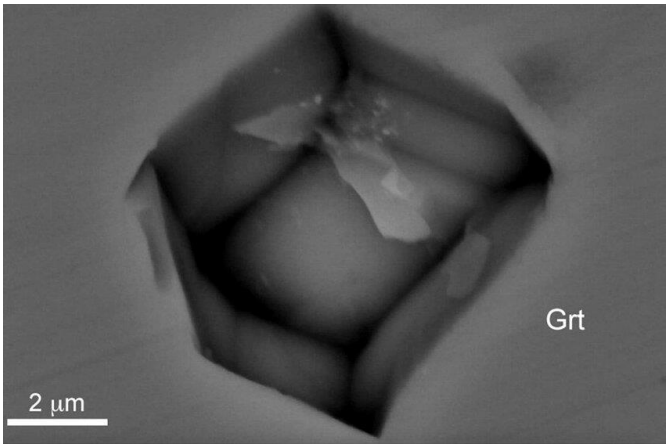

fig. 3.11. Secondary electron SEM image of dodecahedral MI in garnet migmatites from Kali Gandaki (Nepal) (Cesare et al. 2015).

3.3.1 Analytical Techniques to Investigate Nanogranitoids

Nanogranitoids are investigated first of all using transmitted and reflected light optical microscopy in order to recognize which inclusions are birefringent and multi-phases and what are not.

Once detected, and observed by SEM imaging, nanogranitoids must be re-homogenized in order to recover complete compositional data. Two different experimental approaches can be used for this purpose: 1) the heating stage at room pressure and 2) the piston cylinder apparatus under confining pressure. The former has an important disadvantage that is the likely generation of large overpressure in the MI with their subsequent decrepitation and loss of volatiles during remelting experiments (Cesare et al. 2015). The piston cylinder technique overcomes the previous problem imposing a confining pressure during experiment, but it takes much more time (see chapter 4 for piston cylinder apparatus description) (Bartoli et al. 2013).

Re-homogenized MI can be analysed for a lot of elements. Major elements are commonly investigated using electron microprobe (EMP). The content of H_2O and CO_2 can be quantified on re-homogenized MI using different techniques reviewed

by Cesare et al. (2015): Raman spectroscopy (Bartoli 2013; Ferrero 2015), second ion mass spectrometry (SIMS) (Chupin 2006) and NanoSIMS (Bartoli et al. 2014; Carvalho et al. 2018). Trace element contents in MI can be analysed using LA-ICP-MS (Acosta-Vigil et al. 2010; Cesare and Acosta-Vigil 2011).

Chapter 4. Analytical and Experimental Methodologies

Preliminary petrographic and microstructural observations have been made using thin (30μm) and thick (200-300μm) sections under transmitted and reflected light optical microscopy, respectively.

A more detailed study on the nature of inclusions was performed by Scanning Electron Microscope (SEM) obtaining, in addition to specific microstructural observations, semi-quantitative chemical microanalyses. This part was carried out with a CamScan MX 3000 - SEM equipped, micro-chemical analyser (EDAX) and filament in lanthanum hexaboride (LaB_6) at the Department of Geosciences, University of Padua. Eight mounts were prepared to investigate the samples Valp3a, Valp 3b, Valp 6, Valp 8b, Valp 11, Valp 12bis, Valp 13. They were polished and finally coated with a graphite film, with the aim of collecting first of all electron backscattered images (BSE) for the microstructural study of inclusions and their areal distribution in the garnet, and subsequently the semi-quantitative analyses of the different phases within the same inclusions through the EDAX system.

The chemical analysis of the host crystal was performed using an electron microprobe (EMP) along two transects of two garnets from samples Valp 11 and Valp12_bis. Both transects cross the longest section of garnets, passing through their cores. I used a Cameca SX50 microprobe of the CNR-IGG at the Department of Geosciences, University of Padua, with 20 kVolt beam acceleration, 20 nA current, acquisition time at the peak of 10 seconds and 5 seconds on the background. Samples were prepared in two 1-inch mounts, and were perfectly polished to eliminate any roughness. Subsequently, the surface of samples was made conductive in order to discharge the electron beam and to reduce the effects related to electrostatic charges. For this purpose, they have been coated (i.e., covered by a conductive material) depositing a very thin (200 Å) film of graphite on the sample surface by thermal evaporation at high vacuum conditions.

Re-melting experiments of polycrystalline inclusions have been carried out with the aim of homogenizing inclusions at controlled pressure and of preventing inclusion decrepitation. Experiments were performed at the Experimental Petrology Laboratory of the Department of Earth Sciences, University of Milan, using an *end-loaded piston cylinder apparatus* (fig. 4.1).

fig. 4.1. End-loaded piston cylinder at Department of Earth Sciences, University of Milan.

Fragments of garnet (chips) were used for these experiments. They had a variable thickness of 200-300μm and they were obtained from the thick sections observed

with transmitted light microscope. Two different preparations were adopted. In both experiments three garnet portions having size about 2mm were introduced into a gold capsule (99% Au) with an external diameter of 3mm. In the first experiment, chips were isolated from each other with silica powder while in the second one I used graphite. Totally I analysed two gold capsules that contain three garnets each, from the same sample Valp11.

Thanks to an argon welding, the capsules were sealed and were inserted into a sample holder made of MgO salt, enclosed by graphite, pyrex glass and finally a NaCl sleeve (fig. 4.2).

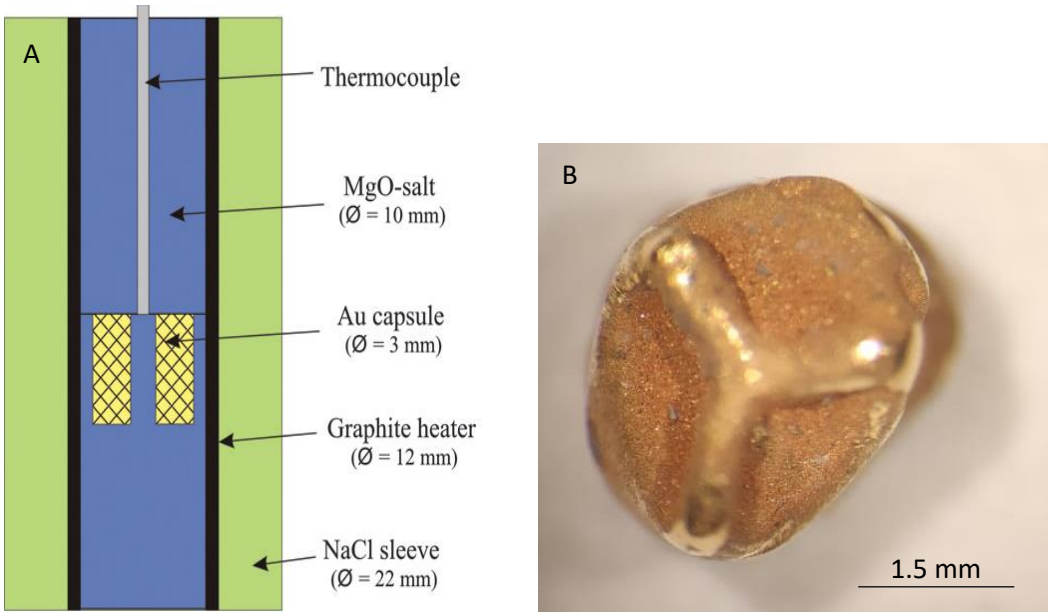

fig. 4.2. Schematic representation (A) of all parts that form the experimental assembly. Garnets are into the gold capsule (Bartoli et al. 2013)*. The image (B) shows the welding of a gold capsule bottom prepared for this study (External diameter of 3 mm).*

The first experiment, with silica powder to isolate garnets, was conducted increasing pressure until 10 kbar at room temperature. Subsequently, when the apparatus was stabilized at the target pressure, the temperature was increased up to 800°C with steps of 50°C per minute.

The experiment was maintained at conditions of 10 kbar and 800°C for 24 hours. The temperature was controlled by a K-type thermocouple with an accuracy of ± 5°C. The gold capsule was subsequently removed and incorporated in an epoxy resin. The obtained pad has been manually polished with the use of 1200, 2400, 4000 mesh abrasive sheets mounted on a rotating plate.

fig. 4.3. BEI SEM image of the assembly of the first experiment of Valp11. Three chips of garnet are loaded into gold capsule along with silica powder.

The second experiment was carried out in the same way as the previous one, but the target temperature was 850°C. Once finished, the gold capsule was immersed in a turpentine solution (5 ml of nitric acid + 15 ml of hydrochloric acid) to dissolve gold. The residuum so obtained was washed in distilled water (for 20 minutes) and dried at room temperature. Subsequently, I manually picked the garnets fragments from the graphite using a brush and ethanol, with the support of a stereoscope, with

the purpose to clean as much as possible the garnets from the graphite powder. Once isolated, garnet fragments were incorporated in epoxy resin and polished (fig. 4.4).

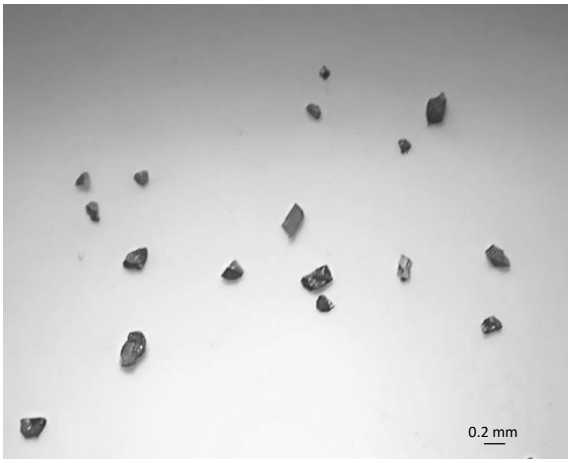

fig. 4.4. Fragments of garnet after the second experiment.

Chapter 5. Petrography and Microstructures

5.1 Petrography

The 101 samples collected during the field activity have been cut and a total of 77 thin sections have been prepared. All the thin sections have been carefully observed under the optical microscope to retrieve the major number of samples showing potential polycrystalline inclusions. Three samples have been selected for a subsequent work of microstructural and microchemical characterization. These samples are Valp6 and Valp8b collected at WPT 006 and Valp11 from WPT 007 (see tab. 2.1).

5.1.1 Valp6

The mineral assemblage of Valp6 is quartz + biotite + garnet + plagioclase ± K-feldspar ± sillimanite and also there are some accessory phases rutile ± graphite. The thin section shows a porphyroblastic structure and an alternation of melanocratic and leucocratic layers can be recognized (fig. 5.1).

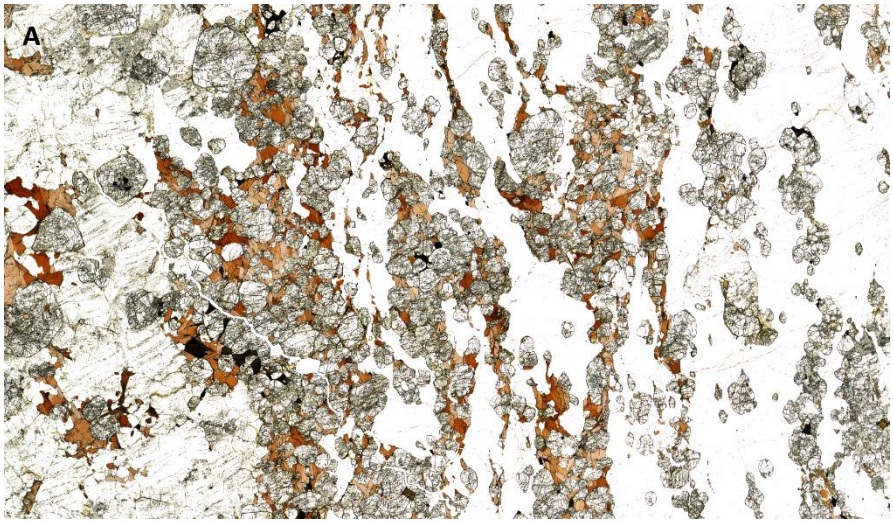

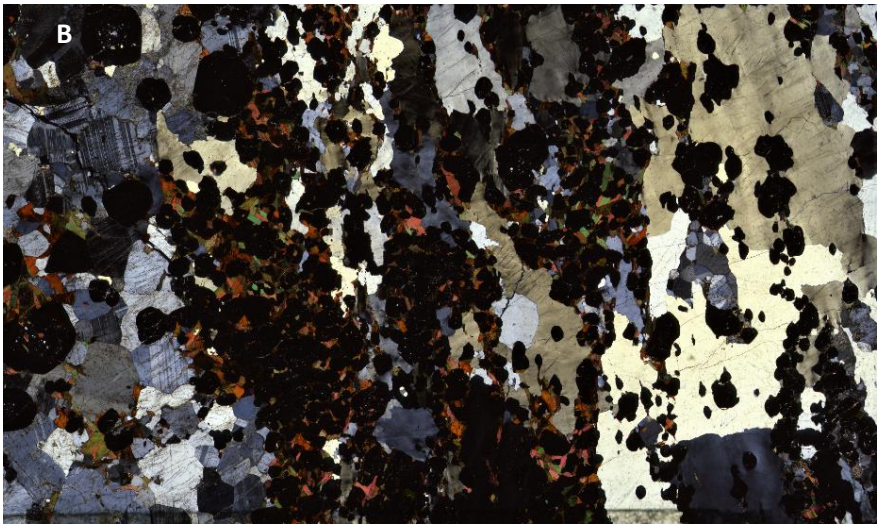

fig. 5.1. The entire thin section under plane-polarized light microscope (A) and crossed-polarizers mode (B) (long side = 3.8 cm).

Biotite occurs as idiomorphic lamellae with rectangular sections. The pleochroism is marked and the colour varies from pale yellow to red-brown (fig. 5.2). Crossed-polarizers observations show brown and green interference colours. There is sometimes chlorite as alteration product.

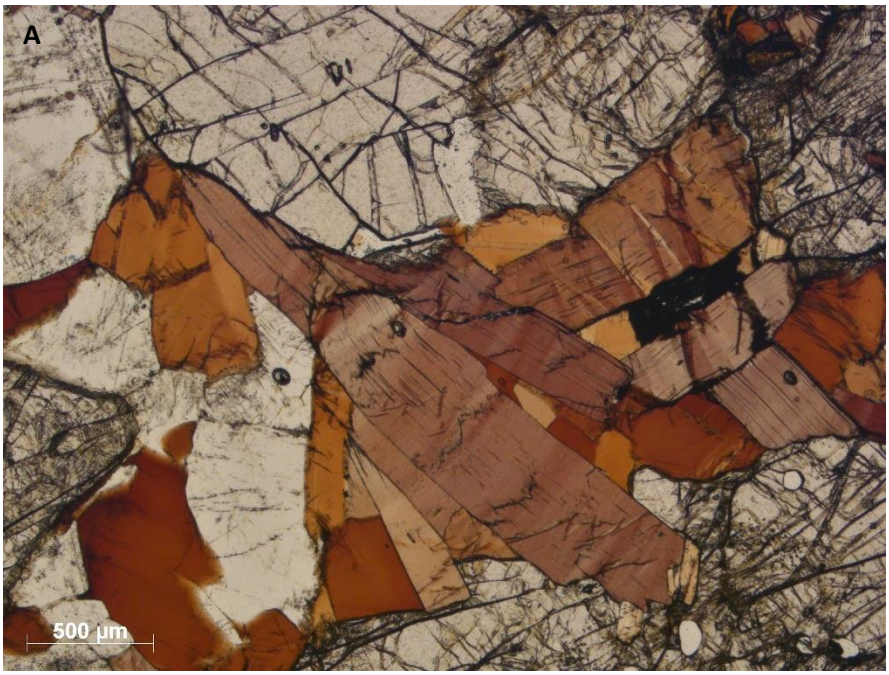

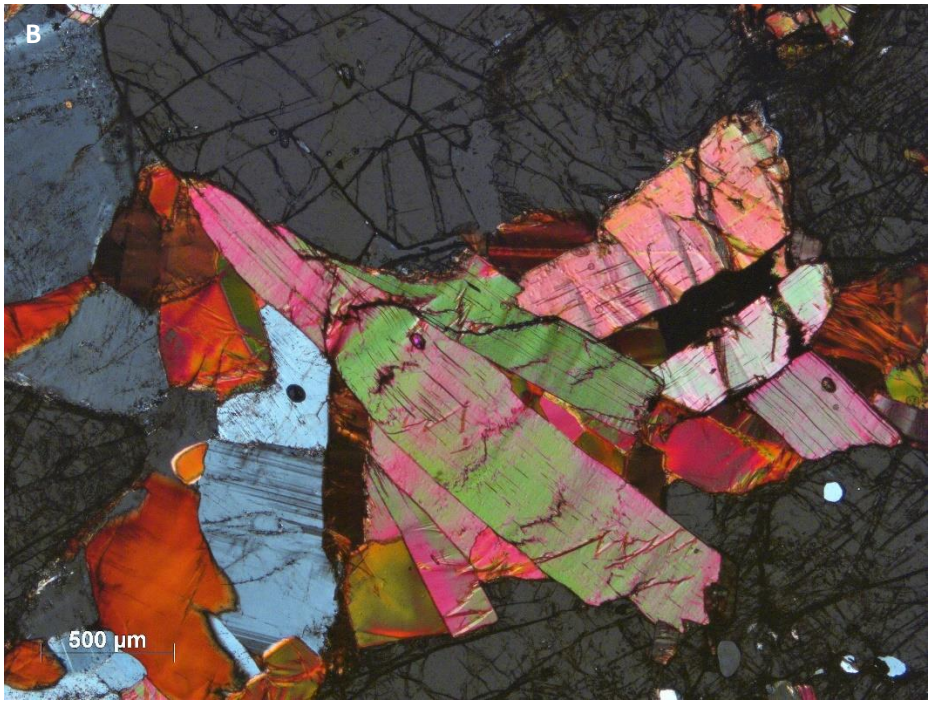

fig. 5.2. Photomicrograph (A) shows the pleochroism of the biotite in this sample. Plane-polarized light. (B) is the same image but under cross polarized light.

Quartz is concentrated in the leucosome of the sample and it occurs as coarse crystals. Quartz can host some inclusions of sillimanite.

In the leucosome some crystals of quartz have lobate boundaries, and this feature testifies for a crystallization from a melt (fig. 5.3).

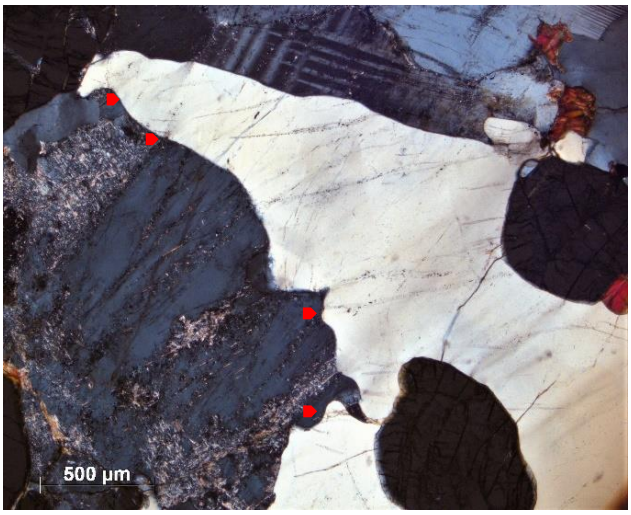

fig. 5.3. Lobate boundaries of quartz signed by red arrows.

Feldspars are weakly altered into sericite. They are abundant in the more leucocratic layers associated to the quartz (fig. 5.4 and fig. 5.6).

Rutile is present as accessory mineral. It has high relief and light brown-dark yellow colour (fig. 5.5).

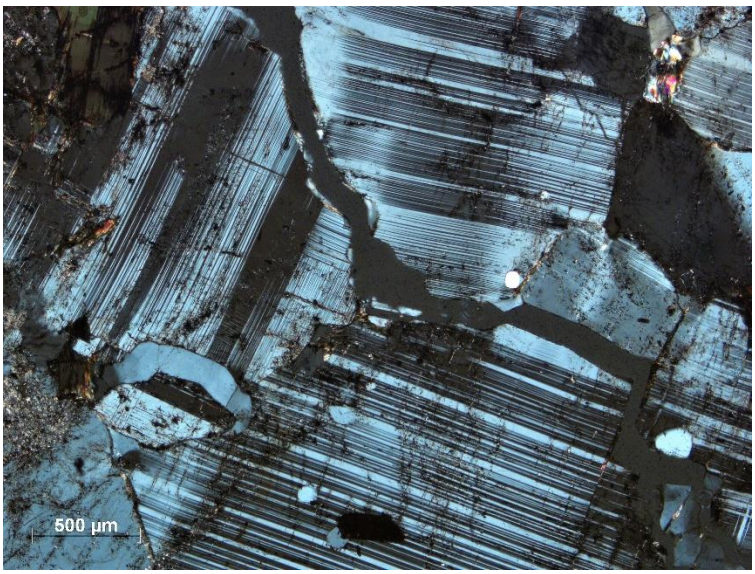

fig. 5.4. Zoned plagioclase with alteration of sericite.

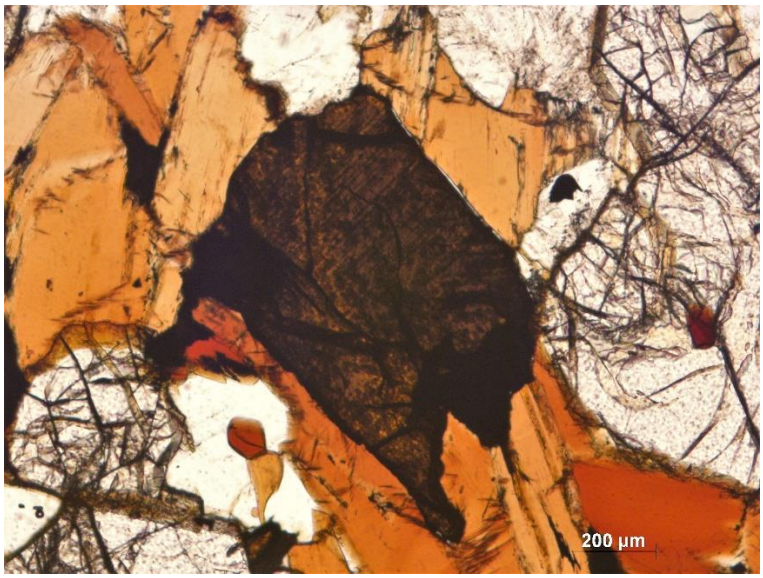

fig. 5.5. Rutile crystal associated with biotite.

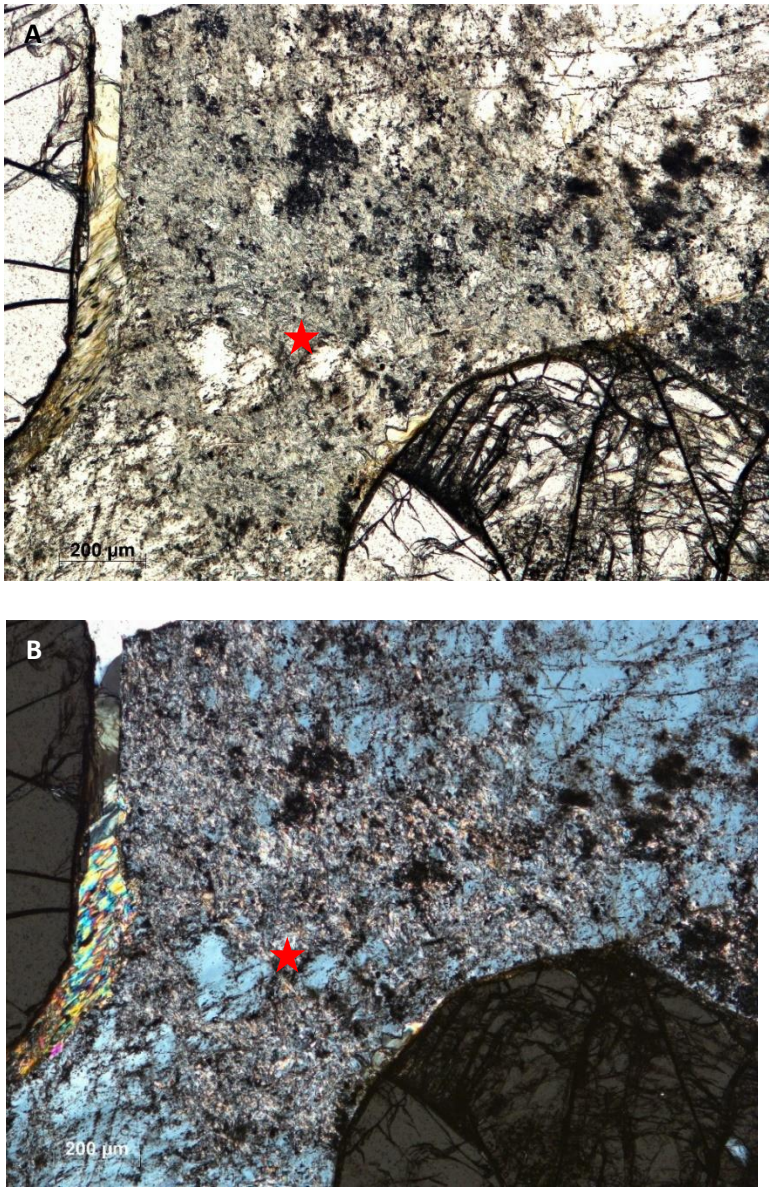

fig. 5.6. Intense sericite alteration under parallel (A) and cross polarized light (B) respectively. Red star indicates sericite.

Garnet is the most abundant mineral in the thin section. The diameter of crystals varies from 600 µm to 2500 µm. Some fractures are present and sometimes crystals are altered. Garnets can host a lot of inclusions of sillimanite (fig. 5.7), quartz, biotite and opaque minerals (fig. 5.8).

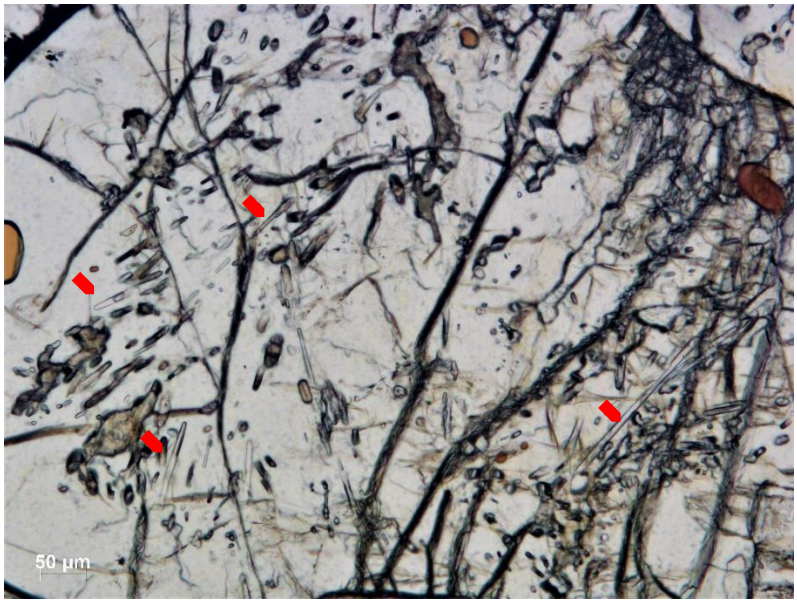

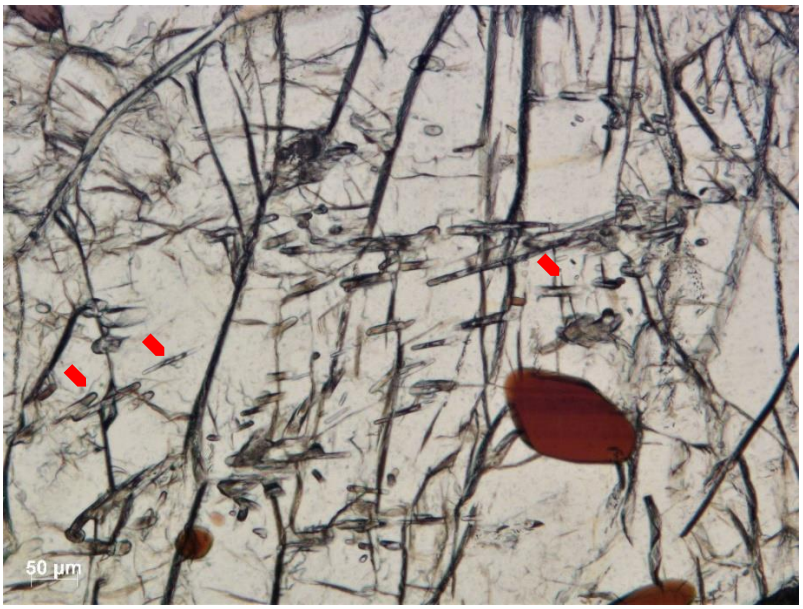

fig. 5.7. Two different crystals of garnets that contain inclusions of sillimanite. Red arrows indicate sillimanite.

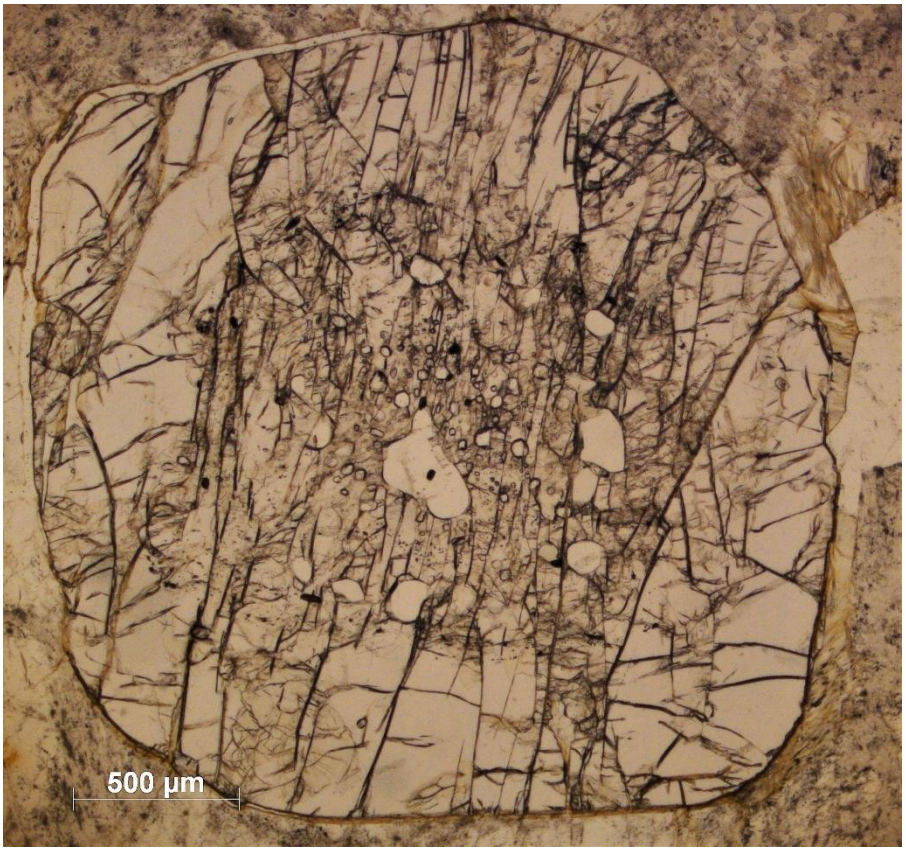

fig. 5.8. Idiomorphic fractured garnet rich of inclusions. The red arrows indicate inclusions of quartz.

5.1.2 Valp8b

The mineral assemblage of Valp8b is garnet + quartz + plagioclase + biotite + sillimanite ± K-feldspar. Rutile and graphite are present as accessory phases. It corresponds to the mineral assemblage of a typical *kinzigite*, even if sillimanite is not very abundant. The sample shows a granoblastic structure and isotropic texture with a feeble evidence for a layering made of melanosome formed by garnet + biotite and leucosome formed by quartz + K-feldspar + plagioclase ± sillimanite (fig. 5.9).

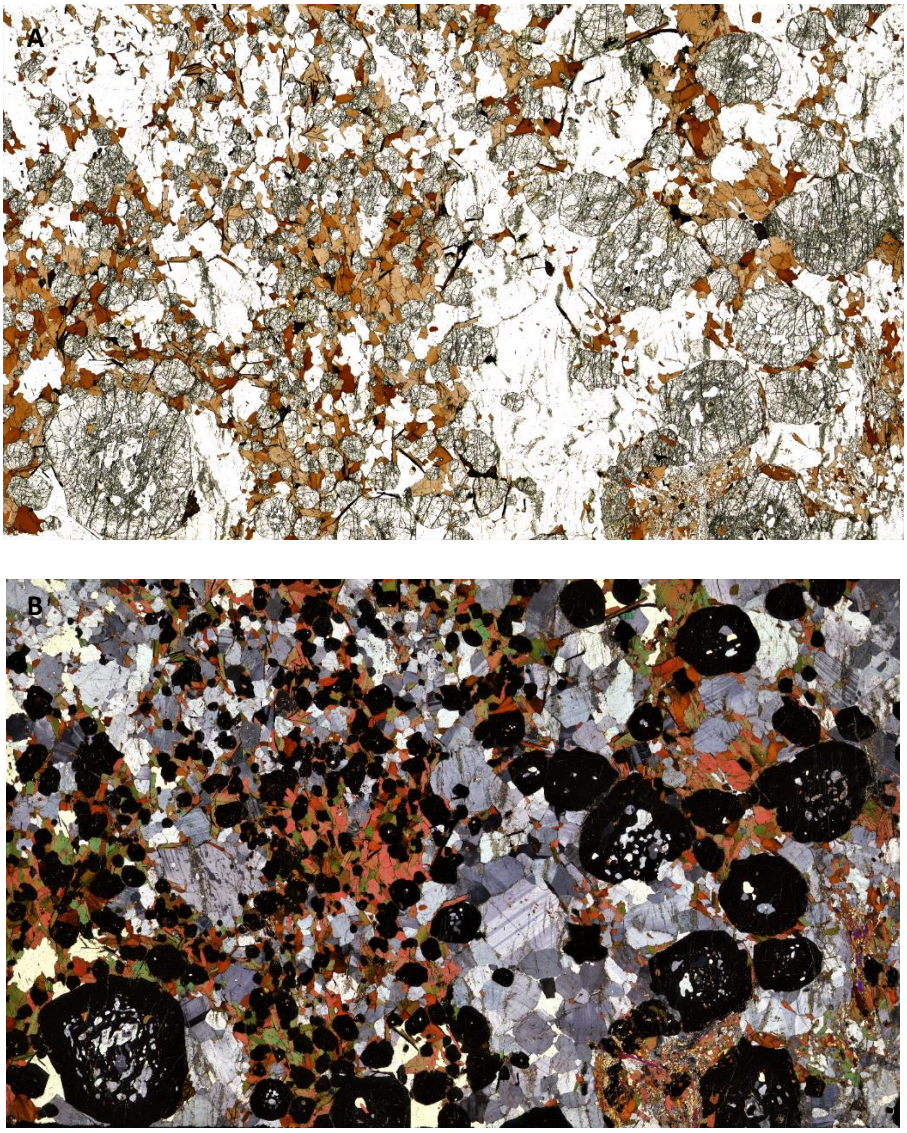

fig. 5.9. The entire thin section under plane-polarized light microscope (A) and crossed-polarizers mode (B) (long side = 3.8 cm).

Biotite shows idiomorphic crystals with and rectangular sections. It often surrounds garnet. The pleochroism is marked and the colour varies from pale yellow to red-brown. Crossed-polarizers observations show the interference colour range from green to red. Graphite is often associated with biotite, in coarse lamellae or aggregates of smaller crystals (fig. 5.10).

fig. 5.10. (A) and (B) are respectively parallel and cross polarizers microphotographs of biotite surrounding garnet. One can observe the pleochroism of the minerals. Red arrows indicate graphite. The yellow arrow indicates rutile.

Feldspars are associated with the leucosome of the thin section (fig. 5.11 and fig. 5.12). Sericite is sometimes present as alteration product of plagioclase.

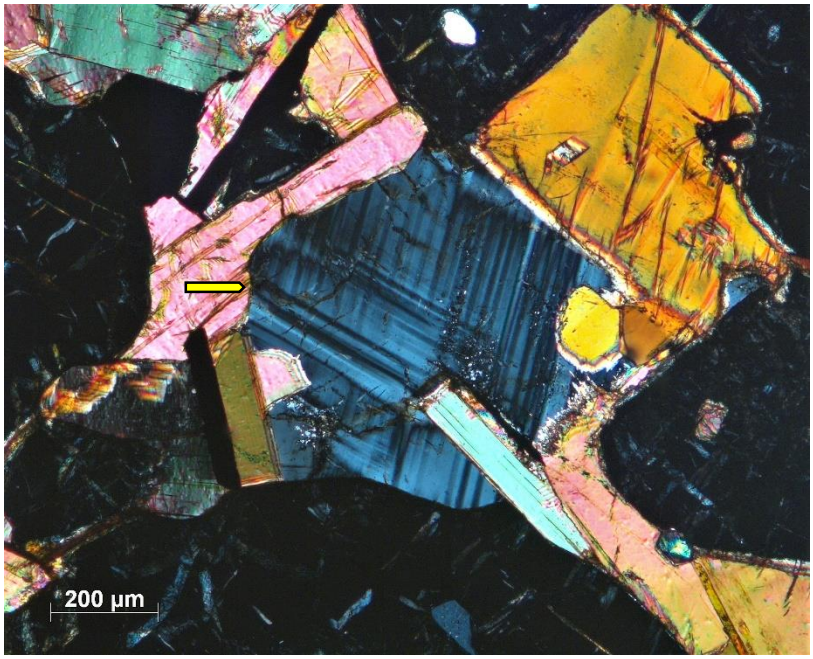

fig. 5.11. K-feldspar crystal indicated by yellow arrow.

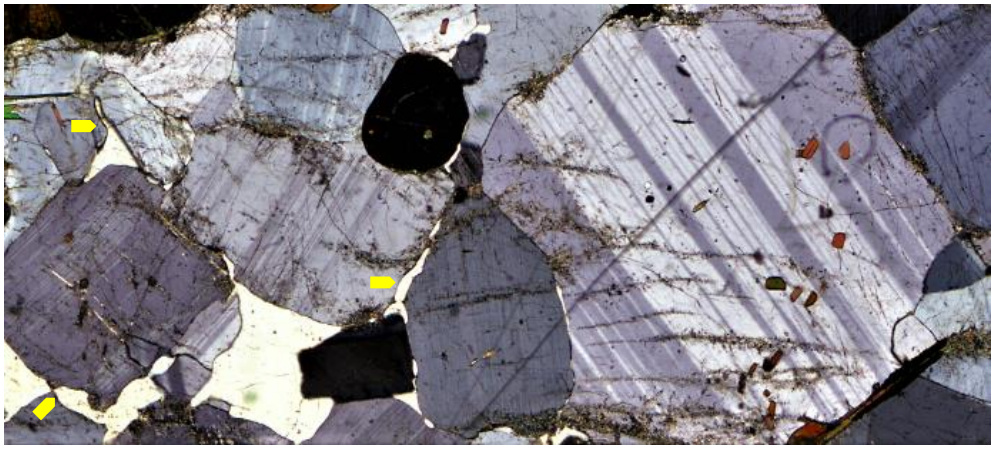

fig. 5.12. A leucocratic mineral assemblage in the leucosome with quartz + plagioclase + sericite alteration. The view shows also well developed pseudomorphs after melt films indicated by yellow arrow.

Sillimanite shows elongated and prismatic crystals. It is colourless and using crossed-polarizers it has maximum 2nd-order interference colours (fig. 5.13)

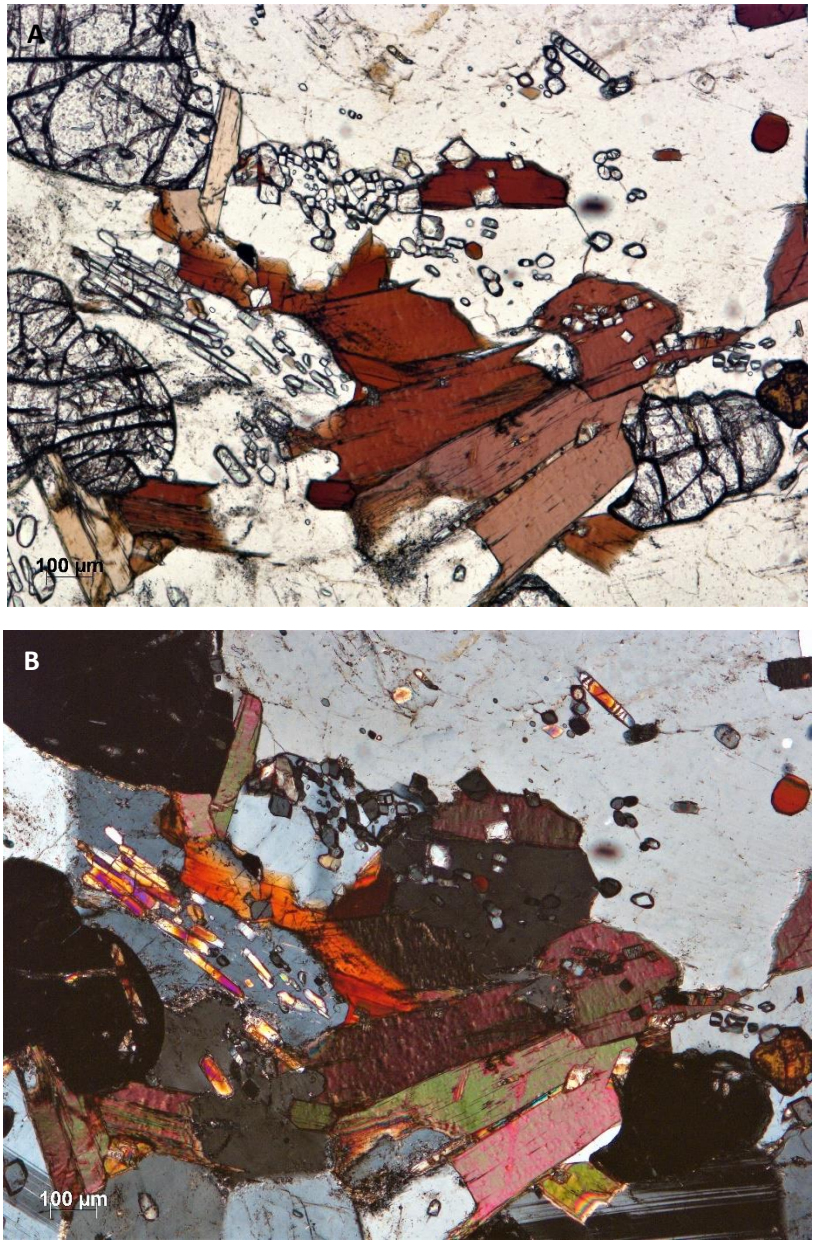

fig. 5.13. Sillimanite crystals included in plagioclase, garnet and quartz. A: plane polarized light; B: crossed polarizers.

Garnet size varies from 700 µm to 5000 µm. Garnet is colourless and it is concentrated in the melanosome part of the section. Garnet is fractured and the majority shows euhedral crystal shape.

Garnet contains a lot of inclusions of quartz and biotite (fig. 5.14).

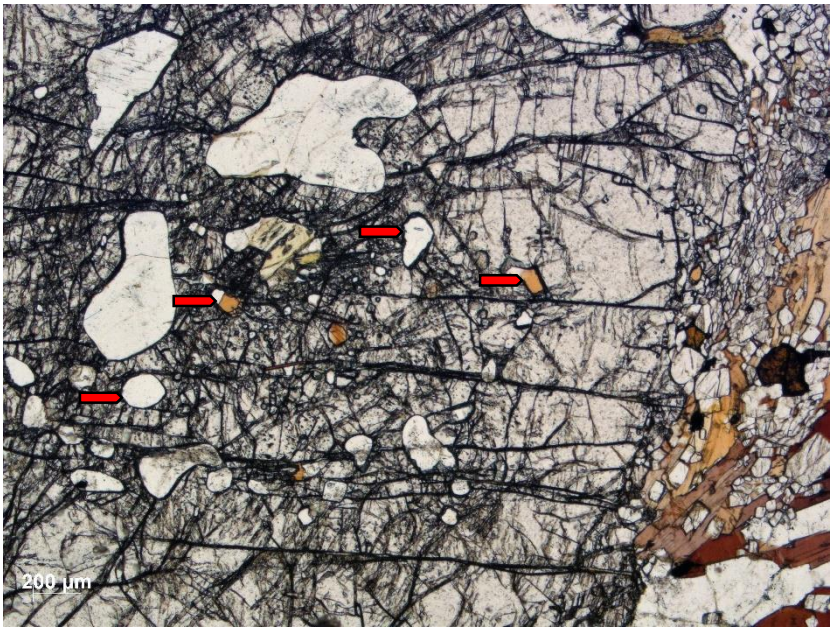

fig. 5.14. Severely fractured and garnet crystal that contains quartz and biotite inclusions indicated by red arrows.

5.1.3 Valp11

The mineral assemblage is garnet + biotite + quartz ± plagioclase ± K-feldspar. Sericite and graphite are present as accessory minerals. The section has a granoblastic structure and is divided into melanosome containing garnet + biotite and leucosome formed by plagioclase + quartz + K-feldspar (fig. 5.15). Garnet is present throughout the sample but the modal amount changes between melanosome, where it is more abundant and leucosome.

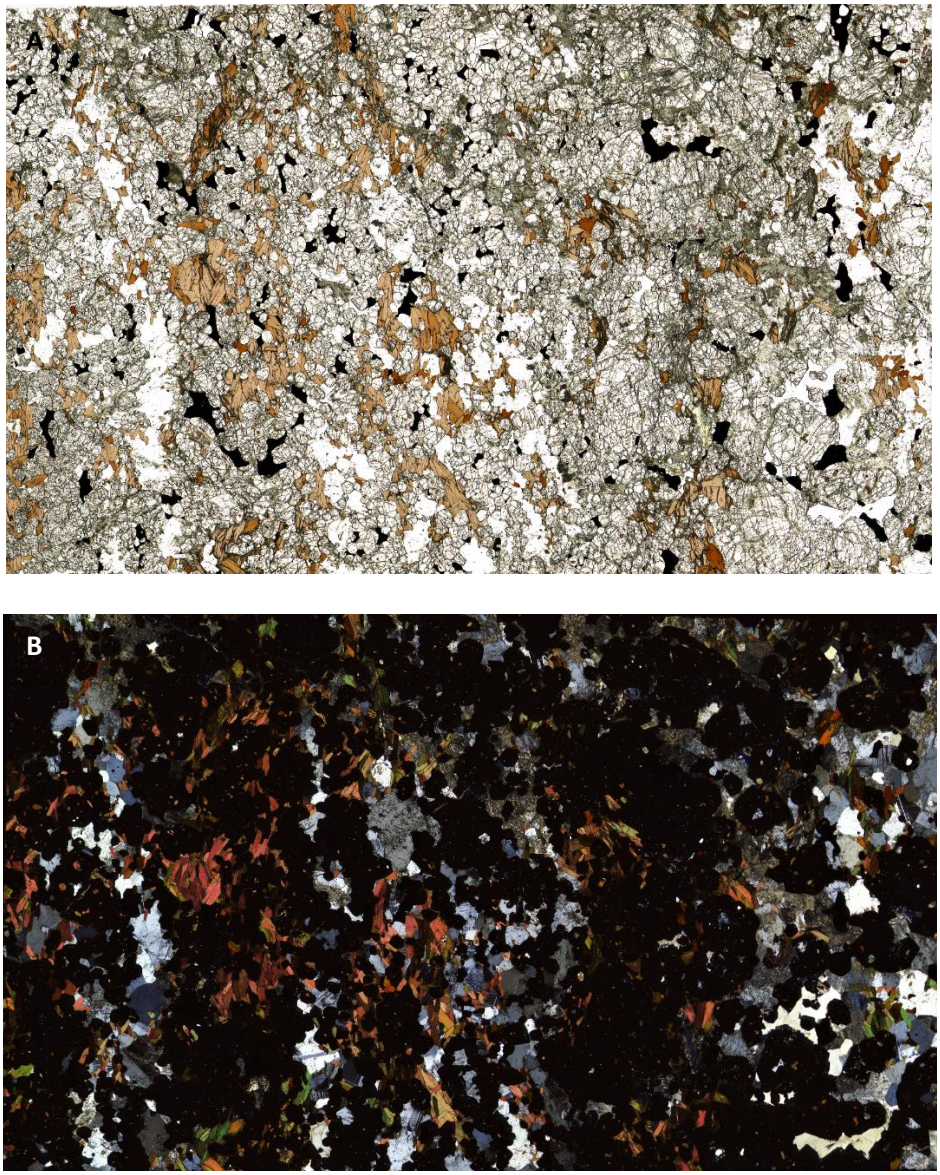

fig. 5.15. The entire thin section under plane-polarized light microscope (A) and crossed-polarizers mode (B) (long side = 3.6 cm).

Biotite occurs as subhedral and tabular grains. The pleocroism is marked and the colour changes from pale-yellow to red-brown (fig. 5.16). Locally, chlorite may replace biotite.

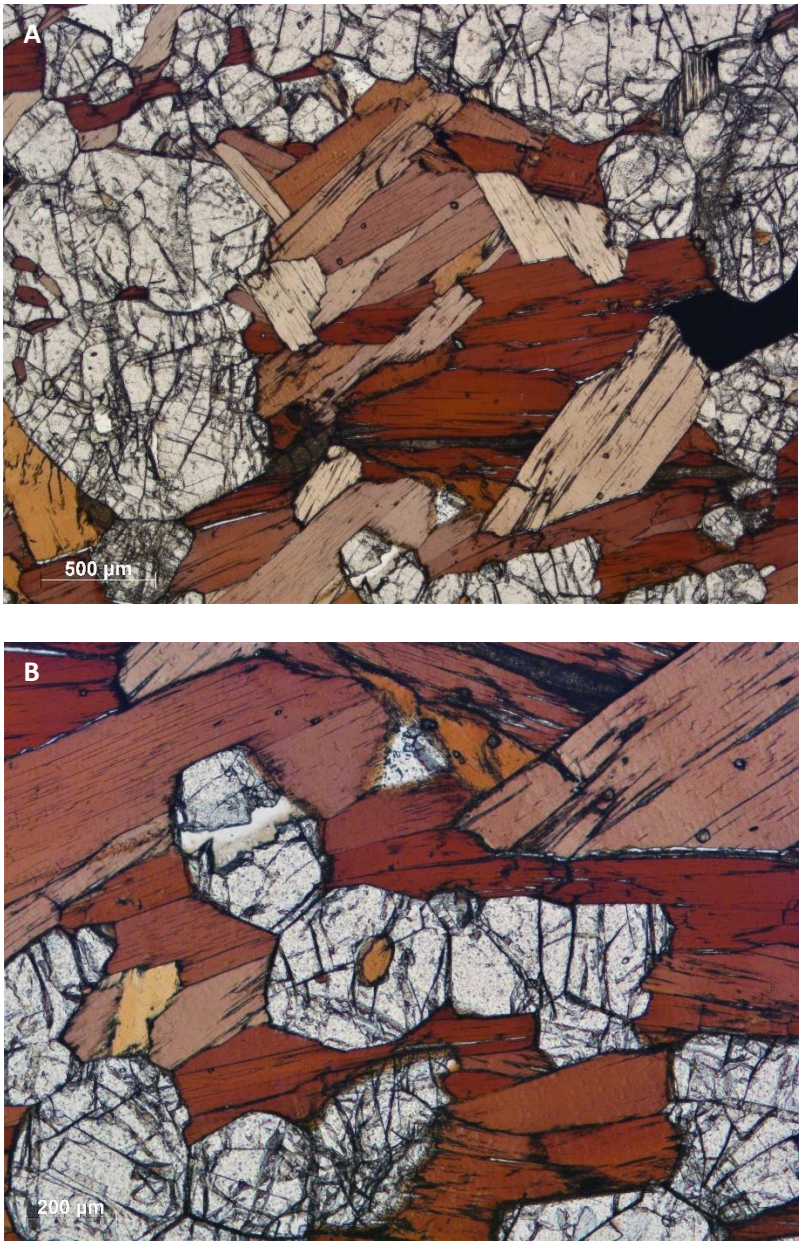

fig. 5.16. A and B show garnet + biotite assemblage forming the melanosome.

Quartz and feldspars are concentrated into the leucosome. Plagioclase may be locally altered in sericite (fig. 5.17 and fig. 5.18).

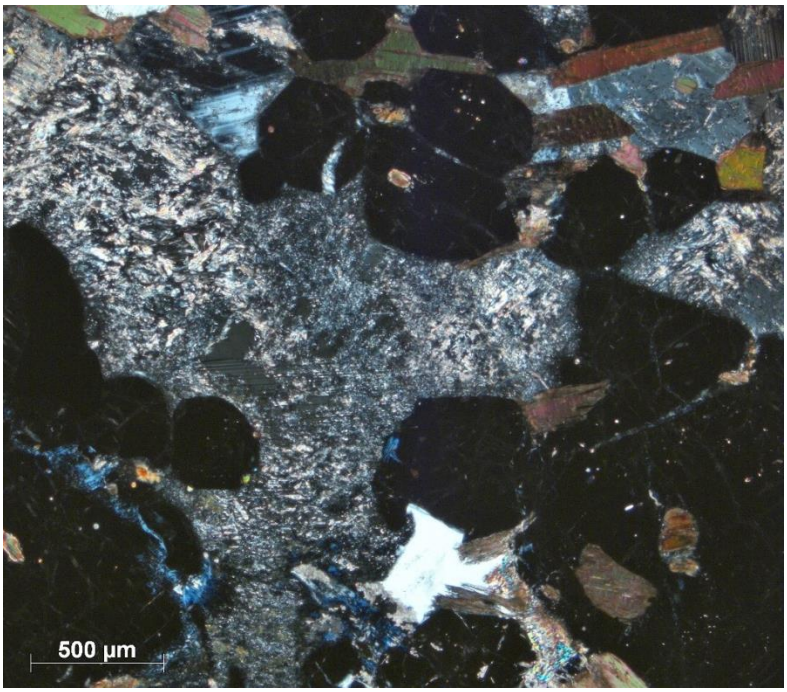

fig. 5.17. Sericite extensively replacing plagioclase.

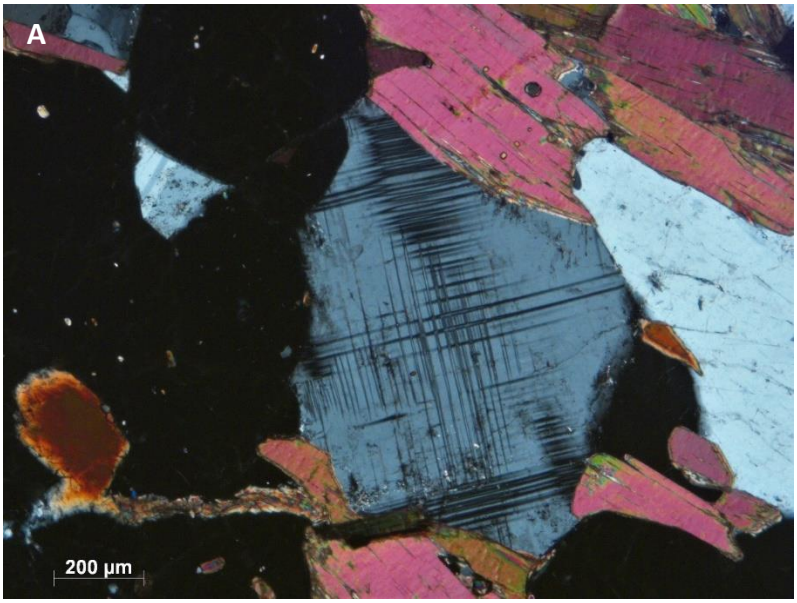

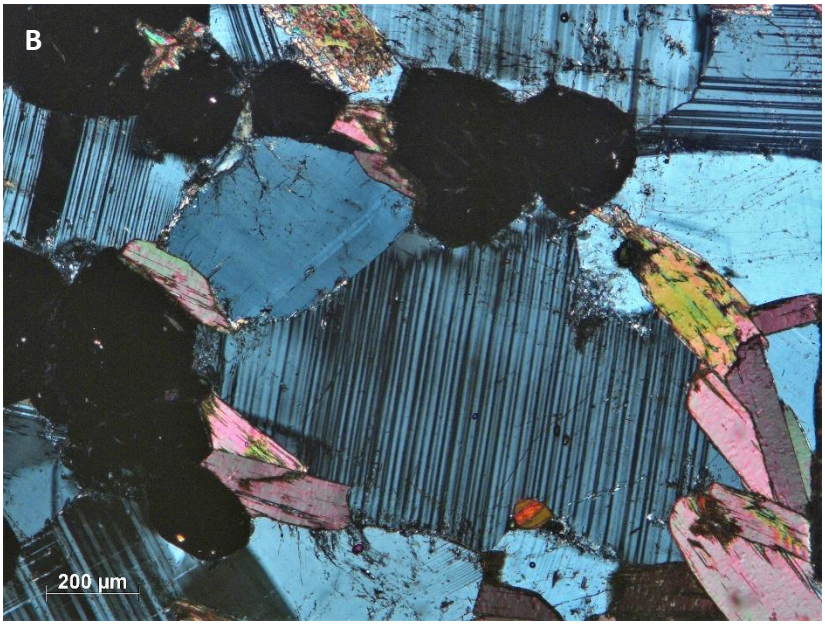

fig. 5.18. A: K-feldspar crystal associated with biotite and garnet. B: part of leucosome of the section with un-altered crystals of plagioclase.

Garnet is the most abundant mineral in the observed thin section. It is isodiametric, colourless and fractured. Garnet hosts mineral inclusions of quartz, biotite and zircon (fig. 5.19). There are also planes of secondary fluid inclusions (fig. 5.20).

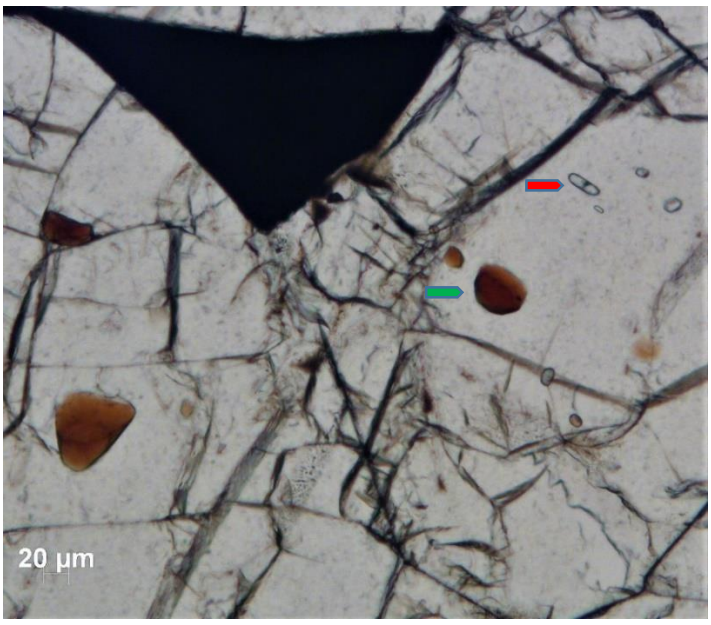

fig. 5.19. The red arrow indicates zircon, the green one biotite.

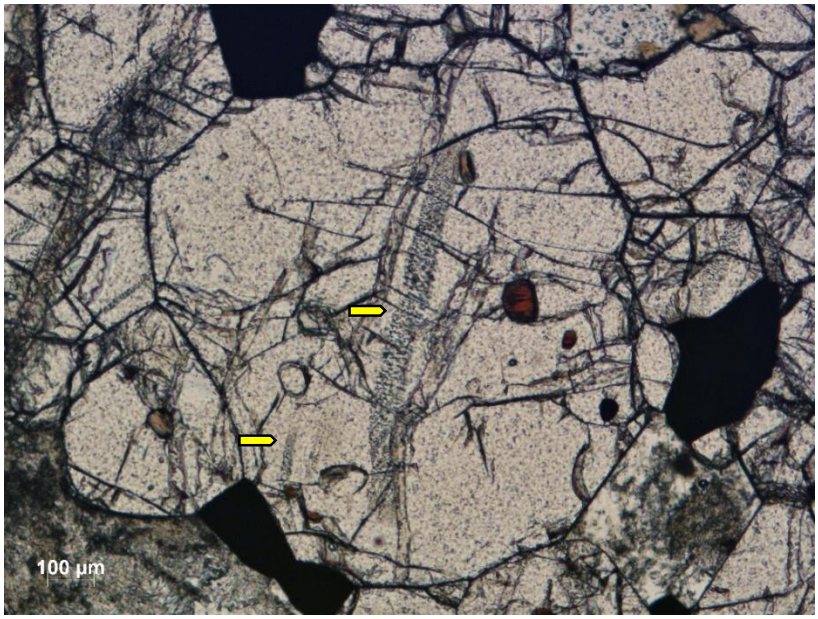

fig. 5.20. Fractured garnet. It is possible to see two planes of secondary inclusions indicated by yellow arrows.

5.2 Nanogranitoid Inclusions

Nanogranitoids appear as brownish inclusions using transmitted light microscopy and the observation under crossed-polarizers allows to identify multiple birefringent crystals within them (fig. 5.21). They are commonly located in the core of the peritectic host garnets (fig. 5.22) and generally show a negative crystal shape with dodecahedron symmetry.

In some clusters, the majority of nanogranitoid inclusions are decrepitated. This is particularly visible under transmitted light where inclusions are characterized by diametrically opposite decrepitation tails (fig. 5.23).

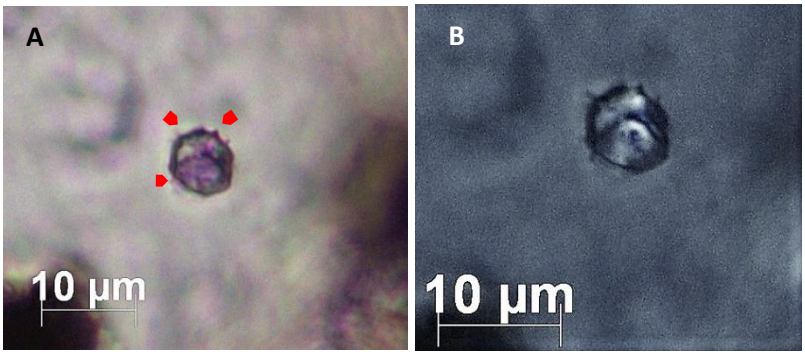

fig. 5.21. Nanogranitoids under parallel (A) and crossed-polarizers (B) containing a polycrystalline assemblage and showing tiny offshoots (red arrows).

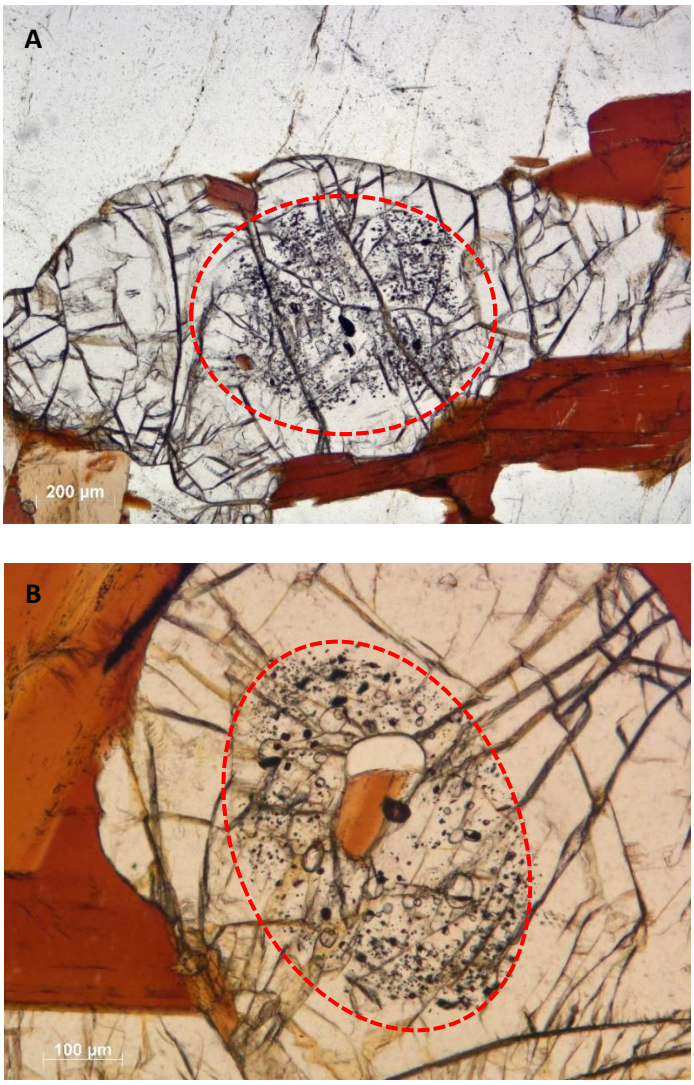

fig. 5.22. Cluster of nanogranites inclusions (dotted red line in A and B) located at the core of the peritectic garnet.

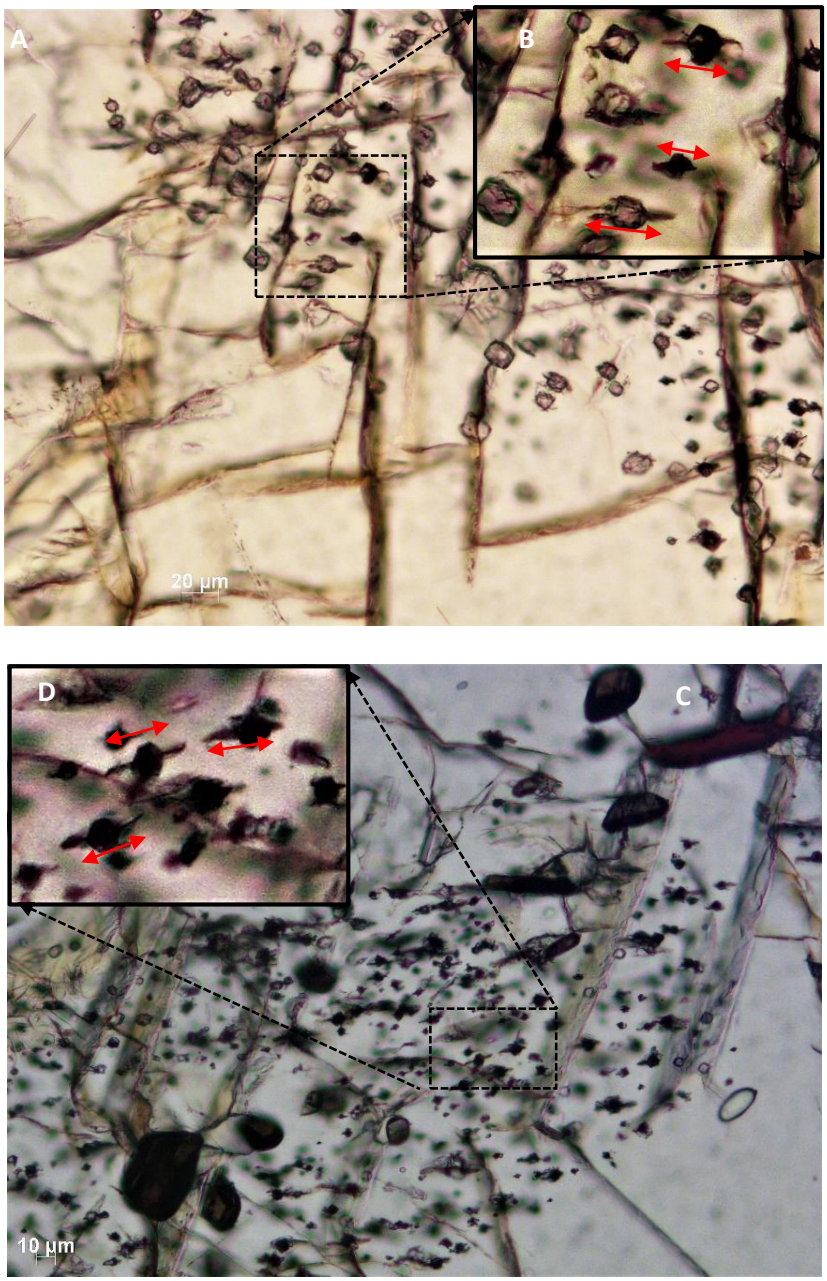

fig. 5.23. A and C show decrepitated inclusions. Red arrows in the close-up B and D indicate the main direction of the offshoots of inclusions.

Inclusions usually contain accessory phases as ilmenite, rutile, apatite and zircon. These minerals are likely accidentally trapped phases (i.e., they were already present when melt was trapped) as suggested by their larger grain size when compared to other crystals; hence they did not crystallize from the melt (fig. 5.24).

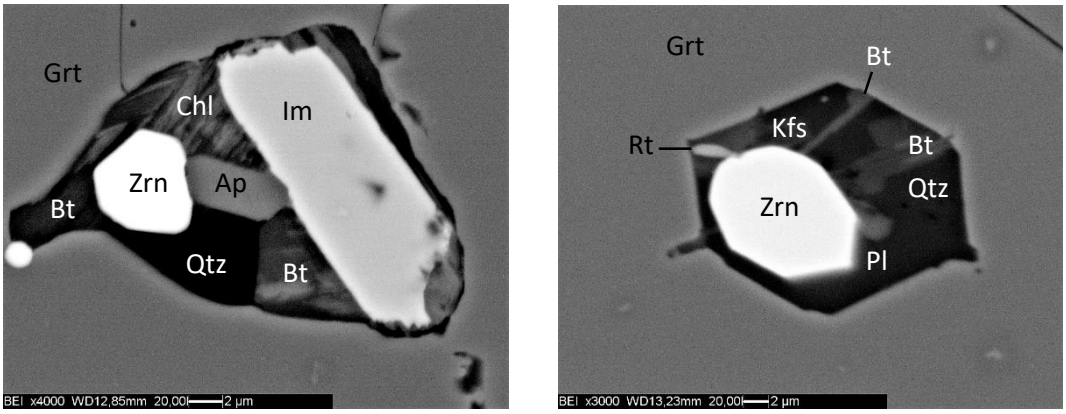

fig. 5.24. BEI SEM images of inclusions with accidentally trapped zircon, apatite, rutile and ilmenite.

Nanogranitoids contain a quartz, K-feldspar, plagioclase and biotite assemblage. Chlorite may be sometimes present associated with biotite. A micro- to nano-porosity occurs in some inclusions (fig. 5.25).

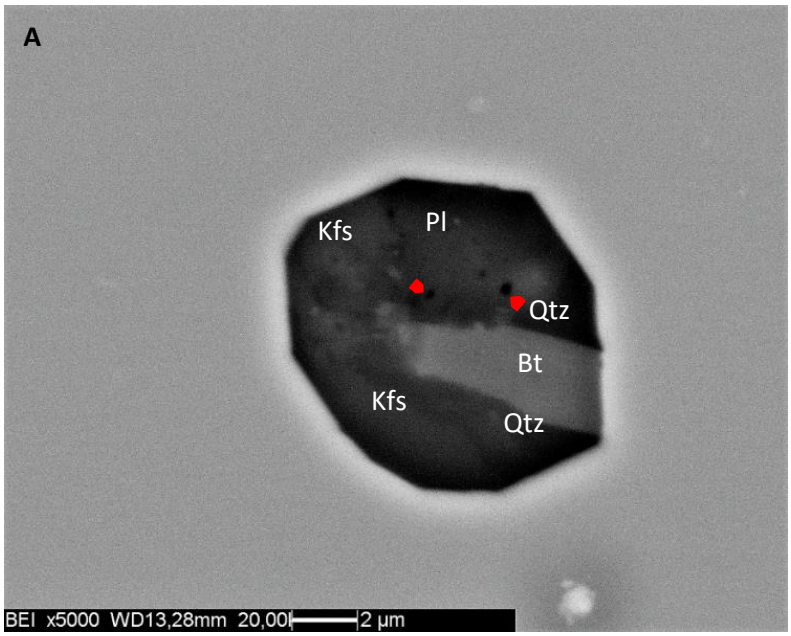

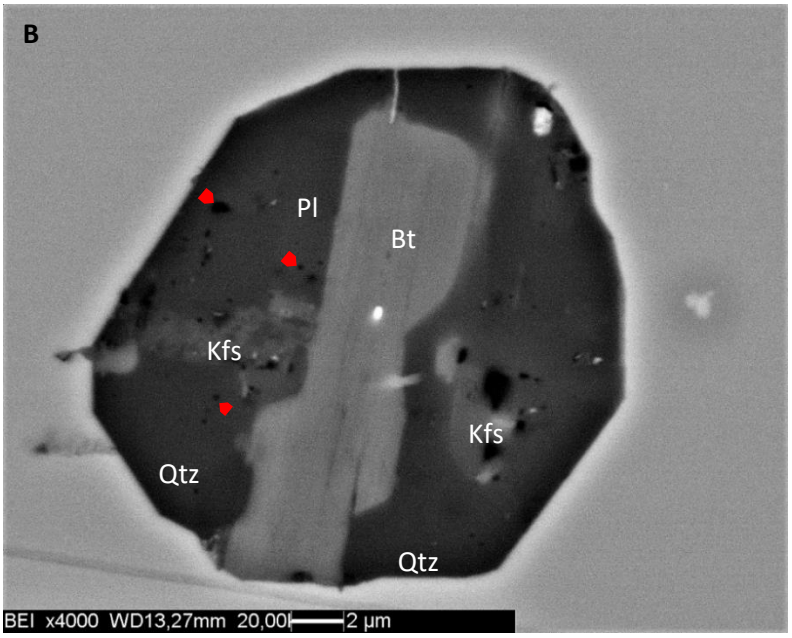

fig. 5.25. BEI SEM images of nanogranitoid inclusions formed by biotite, quartz, plagioclase and K-feldspar. Red arrows in A and B indicate micro- to nano-pores.

5.2.1 Remelting Experiments and Chemistry of the Melt

Nanogranites must be re-homogenized to recover the chemical composition of the trapped melt. Therefore, two remelting experiments using a piston cylinder were run during this study (see chapter 4). The first experiment was conducted at 800 °C and 10 kbar for 24 hours.

At these P-T conditions re-homogenization of inclusions was incomplete or unsuccessful. In fact, nanogranitoids are still totally crystallized or remelted only in part (fig. 5.26 and fig. 5.27).

The inclusion in fig. 5.27 shows evidence of remelting such as the presence of glass (see below), lobate grains and cuspate protrusions of melt.

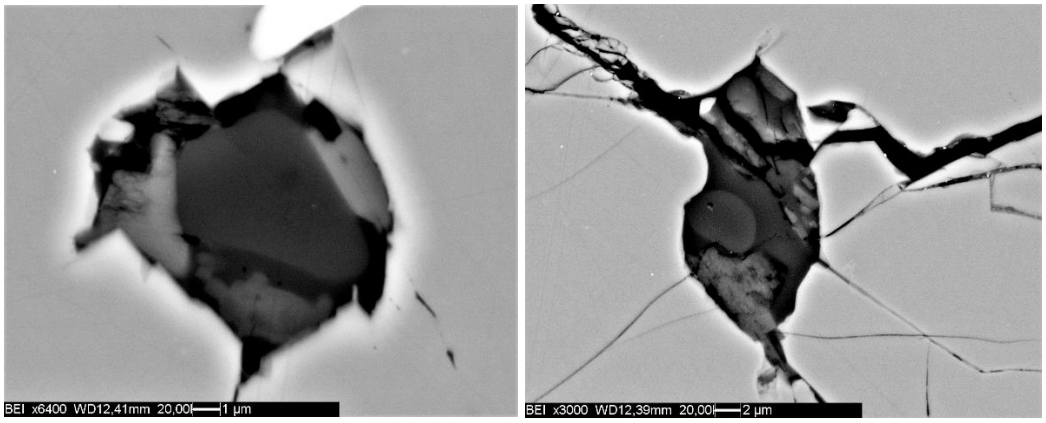

fig. 5.26. BEI SEM images of two different inclusions still containing crystalline phases after the experiment.

Micro-chemical analyses have been made using the EDAX system in order to provide semi-quantitative composition of the different phases in the partially remelted inclusions. In tab. 5.1 the compositions of the phases in fig. 5.26 are reported. A, B, C and D likely represent compositions of a melt showing a certain geochemical variability at the micro-scale, while E probably is a biotite crystal because of the high relative concentration of Fe and Mg. Because the re-homogenization of inclusions was incomplete or unsuccessful, the exact temperature of homogenization has not been reached in the first experiment.

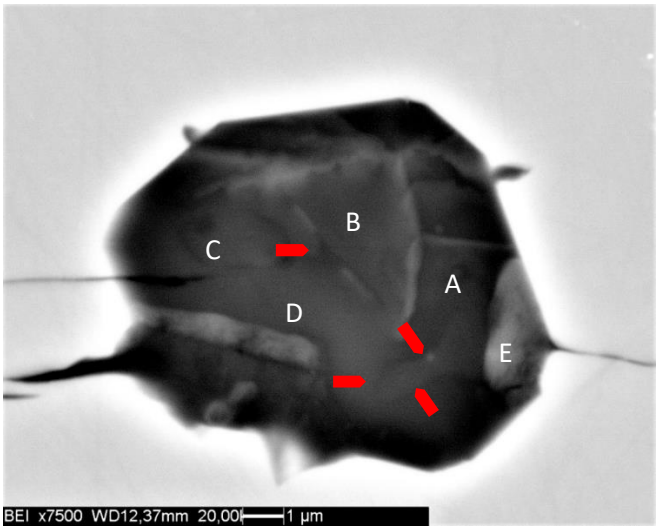

fig. 5.27. BEI SEM image of an inclusion that did not re-homogenize completely. Red arrows indicate structures related the presence of melt such lobate crystals and cuspate protrusions of melt. Each letter corresponds to the same in the tab. 5.1.

	A	B	C	D	E
Na_2O	2.36	2.92	2.84	3.69	1.58
MgO	2.07	1.43	1.53	3.59	9.37
Al_2O_3	11.44	16.88	15.21	18.96	16.75
SiO_2	74.65	68.17	65.55	62.18	49.33
K_2O	3.3	4.16	4.14	4.17	5.93
CaO	2.47	4.71	4.32	2.94	1.61
FeO	3.71	1.73	6.41	4.47	15.43
TOT	100	100	100	100	100

tab. 5.1. Table reports the different semi-quantitative analyses of phases. No volatiles can be detected using EDAX system.

Because nanogranitoids are not re-homogenized at 800°C, the second experiment was conducted at 850 °C and 10 kbar for 24 hours. The inclusions were partially re-homogenized (fig. 5.28). In fig. 5.28 (A) the garnet shows a clear rim due to the interaction with the inclusion during the experiment. In fig. 5.28 (B) the dark part of inclusion is melt. In the lower-left side of the inclusion it is possible to see new crystals that likely crystallized from the wall of the inclusion as result of melt-garnet interaction (red arrows in fig. 5.28 (B)). All these microstructures are indicative of overheating (i.e., the experimental temperature was higher than the temperature of formation).

One inclusion is almost totally re-homogenized after the experiment at 850 °C (fig. 5.29).

Semi-quantitative analysis has been made using EDAX system (tab. 5.2). The phases highlighted as A may be likely a melt considering the low-Fe and Mg concentrations and high SiO_2 content.

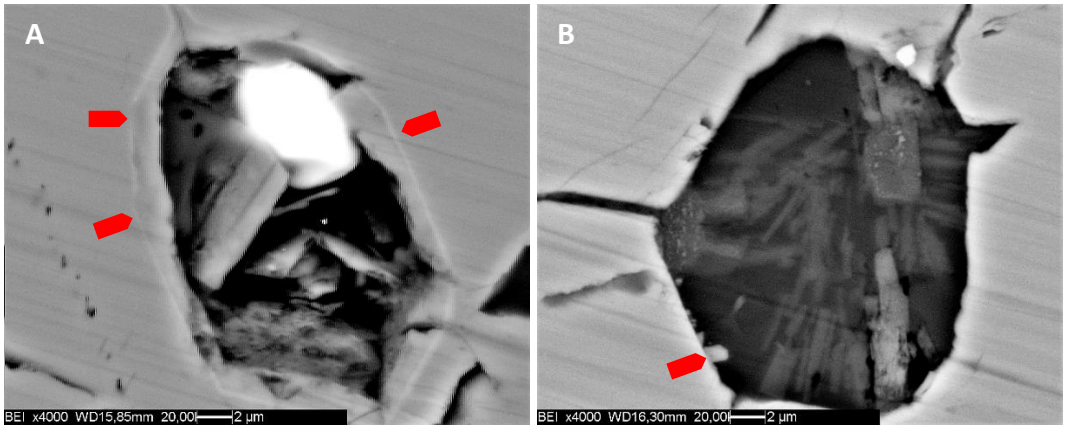

fig. 5.28. A: BEI SEM image showing the different phases inside the inclusion after the experiment at 850 °C. The white mineral is a zircon. The black colour corresponds to holes caused by polishing of the surface of the sample during its preparation. B: BEI SEM image showing different phases in the inclusion. Red arrows show evidence of overheating.

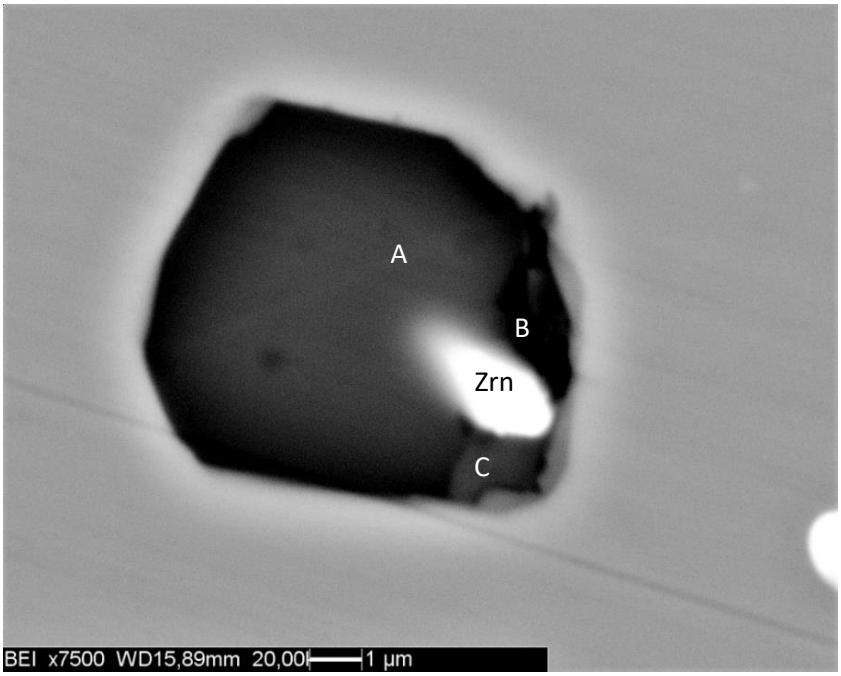

fig. 5.29. BEI SEM showing an almost completely homogenized inclusion. The letters A, B, C correspond to the analyses reported in tab. 5.2.

	A	B	C
Na_2O	2.15	1.85	2.25
MgO	1.64	8.07	13.17
Al_2O_3	13.19	12.33	19.30
SiO_2	71.68	62.71	48.06
K_2O	6.43	4.91	7.07
CaO	0.75	0.86	0.65
FeO	4.16	9.27	9.50
TOT	100	100	100

tab. 5.2. Major element composition of the phases identified by points A, B and C in fig. 5.29.

5.3 Chemical Analysis of the Host Garnet

Chemical analysis of garnet from sample Valp11 has been made using the electron microprobe (EMP) along the transect reported in fig. 5.30.

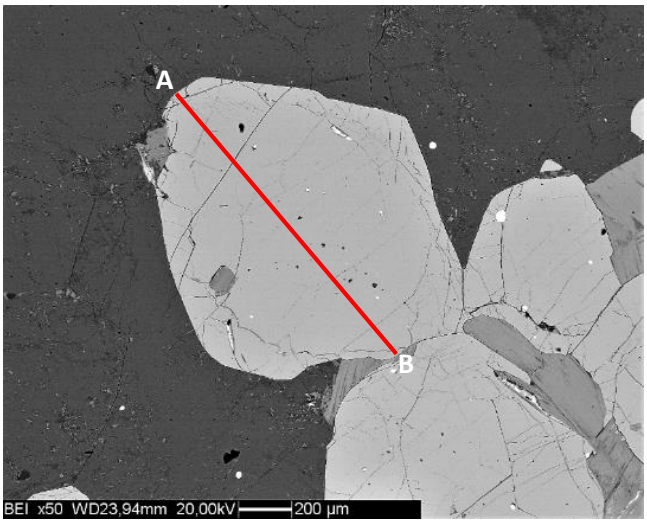

fig. 5.30. BEI SEM image of garnet analysed of the sample Valp11. Red line corresponds to the EMP transect.

The composition of garnet core is $Alm_{60}Pyp_{28}Grs_{9}Sps_{3}$ and the composition of the garnet rim is $Alm_{62}Pyp_{25}Grs_{10}Sps_{3}$ towards the biotite (B in fig. 5.30). The garnet analysed shows a slight compositional zoning, with subtle variations of X_{alm} [Fe/(Fe+Mg+Ca+Mn)] X_{pyp} [Mg/(Mg+Fe+Ca+Mn)] and X_{grs} [Ca/(Ca+Fe+Mg+Mn)] components at the rim toward biotite (fig. 5.31). The amount of X_{alm} and X_{grs} increase towards the biotite while X_{pyp} decreases. In the opposite side of transect, towards the quartz, there are not any variations in composition.

The inclusions are located at the core of the garnet and there are not systematic variations of garnet composition with respect to nanogranitoids occurence.

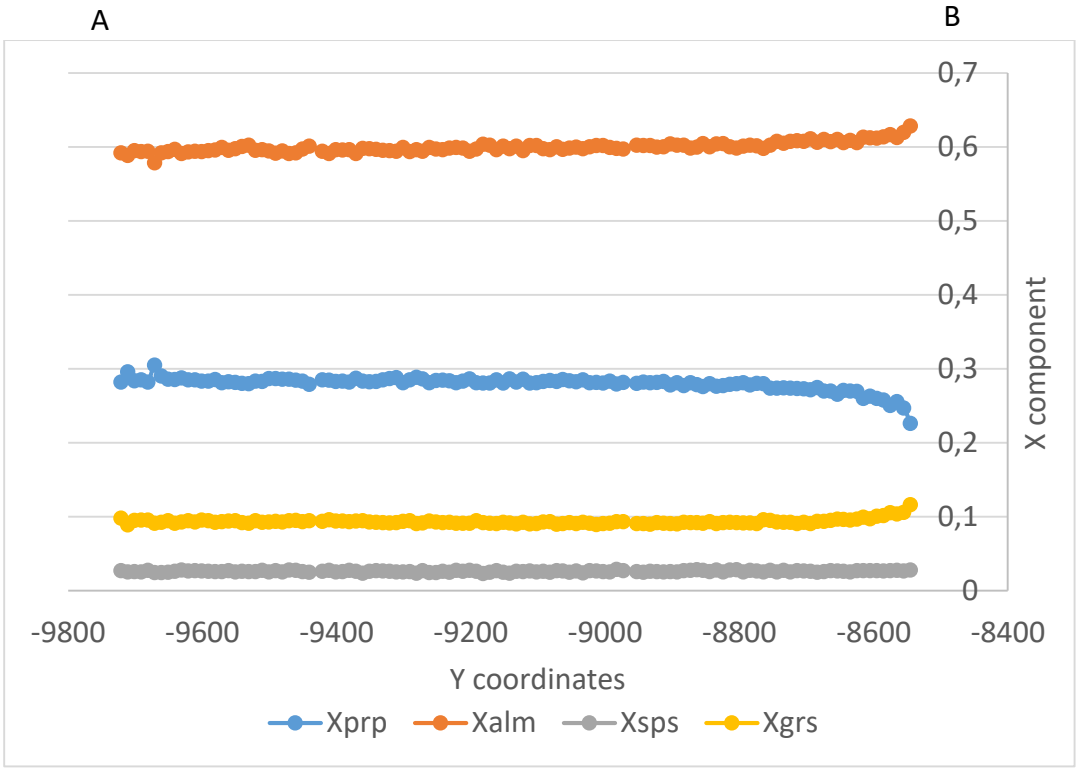

fig. 5.31. Profiles of garnet components measured along the transect reported in fig. 5.30. The letters A and B indicate the boundary with quartz and biotite respectively of the analysed garnet. The results of EMP analysis and all the calculated component are in appendix1.

Chapter 6. Discussion

6.1 Host Rocks

The three samples described in chapter 5 show little differences in the mineral assemblage. Samples Valp6 and Valp8b have the almost typical kinzigite assemblage formed by garnet + quartz + biotite ± K-feldspar ± plagioclase ± sillimanite. Sample Valp11, instead, has garnet + biotite + quartz ± plagioclase ± K-feldspar. The metamorphic peak conditions of the rocks of Valpelline Series are 750-850 °C and 6-8 kbar (Gardien 1994; Manzotti and Zucali 2013; Manzotti et al. 2014). The main difference is probably the composition of the protolith that is more aluminous for Valp6 and Valp8b than Valp11 as testified by the absence of sillimanite both as inclusions in peritectic mineral as mineral in the rock' matrix.

At the outcrop scale, all the samples show evidence of a partial melting. Indeed, Valp6 and Valp8b are collected from a metatexite migmatite (WPT 006 in fig.2.1) and Valp11 derived from a diatexite migmatite located in an amphibolite quarry (WPT 007 in fig. 2.1). At microscopic scale there is evidence of crystallization from a melt as testified by the presence of lobate boundary of leucocratic minerals (fig. 5.3).

The garnet analysed has a composition of $Alm_{60}Pyp_{28}Grs_{9}Sps_{3}$ at the core and $Alm_{62}Pyp_{25}Grs_{10}Sps_{3}$ at the boundary with the biotite. The increase of X_{alm} is possible if retrograde exchange reactions (ReERs) are involved (Kohn and Spear 2000). ReERs do not significantly change the mineral modes and cause divergence of ferromagnesian mineral composition such as in the studied case where garnet becomes more Fe rich while biotite become more Mg rich.

The contact boundary of the analysed garnet with biotite shows also an increases in X_{grs} and this is possible if a Ca-bearing intergranular metamorphic fluid was present between garnet and biotite during the Fe-Mg exchange.

In conclusion, retrograde exchange reactions took place in the studied rocks, probably during the Alpine evolution and deformation. Although the high-grade mineral assemblage was not modified, garnet rims and biotite in contact with them extensively modified their composition by Fe-Mg diffusion, accompanied also by modifications of the grossular content of garnet. these retrograde changes pose serious problems for the application of conventional thermobarometry using garnet rim composition.

6.2 Microstructures of Inclusions and Re-melting Experiments

The inclusions of the analysed samples sometimes show a negative-crystal shape. This feature does not demonstrate their primary origin because it is a post-entrapment change (Maze et al. 1981; Roedder 1984; Sisson et al. 1993; Ferrero et al. 2012). The distribution of MI in the cores of the peritectic garnets testifies their primary origin (i.e., they were trapped during garnet growth)

Nanogranite inclusions display a micro to nano-porosity that probably contained exsolved fluids, in particular H_2O (Cesare et al. 2011). This porosity supports the inference made by Cesare et al. (2009) that porosity forms by melt crystallization due to the higher density of solids with respect to the trapped melt.

The inclusions after the first experiment (800 °C and 10 kbar) were not re-homogenized and some partially remelted inclusions are present. Some of them were decrepitated despite the fact that the experiments were performed under controlled pressure using a piston cylinder apparatus. This is consistent with the abundant decrepitation cracks observed in the inclusion before remelting experiments (fig. 5.22). The most plausible cause is the extensive deformational phase that occurred at the scale of the entire Valpelline unit during the Alpine retrograde path of the host rock. In fig. 5.26, melt structures are visible, testifying the partial melting of inclusions at 800 °C. Given the failure of the first experiment, a second one was necessary at 850 °C and 10 kbar. Some inclusions display

interactions with the host garnet, in particular the formation of a recrystallized garnet-rim around the inclusion, indicating that the trapping temperature was exceeded (fig. 5.28A). The composition of the garnet-rim is probably different from the peritectic garnet because of the different P-T forming conditions. Another consequence of the overheating, is the crystallization on the inclusion wall of a new phase, probably orthopyroxene, as can be observed in fig. 5.28B.

One inclusion has been almost completely re-melted and semi-quantitative analyses have been made on it through the EDAX system. Obviously these analyses do not correspond to the real composition of the anatectic melt, first of all because the inclusion did not completely re-homogenize and secondly because the EDAX system cannot measure content of volatiles and in particular H_2O. The results, however, are representative of an anatectic melt composition, indicating that anatexis if these rocks produced a granitic melts characterized by $SiO_2 \approx 72\%$, $Na_2O \approx 2\%$, $CaO \approx 0.7\%$, $K_2O \approx 6\%$, $FeO \approx 4\%$, $Al_2O_3 \approx 13\ \%$.

The two temperatures that were used for the experiments provide important information to determine the temperature of homogenization of inclusions. The nanogranites inclusions after the first experiment (800 °C and 10 kbar) were partially re-melted and after the second one (850 °C and 10 kbar) they displayed interaction with the host garnet. This indicates that the theoretical temperature of homogenization is between 800-850 °C in agreement with the values of temperature provided by the literature.

Chapter 7. Conclusions

This work has shown for the first time the presence of nanogranite inclusions in the kinzigites of the Velpelline Series. These melt inclusions occur in the core of peritectic garnet and therefore they were trapped during the incongruent melting reaction of this portion of continental crust. Similar occurences have been described in other migmatitic and granulitic terranes worldwide (Cesare et al. 2009, 2011; Ferrero et al. 2012).

This study on melt inclusion from the Valpelline Series, aimed at providing further constraints to the Variscan high-temperature metamorphic evolution in this part of the Austroalpine complex of the western Alps, has suffered some problems and pitfalls. First of all, most nanogranitoids are hosted in garnet grains showing a high degree of microfracturing and, as a consequence, many decrepitated inclusions have been found. For this reason, many samples (101) have been collected during the field activity and the thin sections have been subjected to a preliminary selection to find analysable nanogranites. Another difficulty is related to the small size of some inclusions. For example, from the samples Valp6 and Valp8b a lot of inclusions were not workable because of their very small size (< 2 μm). As a consequence, the number of samples suitable for a re-homogenization study has turned out extremely limited.

Re-melting experiments have been made using a piston cylinder apparatus in order to homogenise nanogranites preventing or minimizing their decrepitation. After the first experiments at 800 °C and 10 kbar for 24 hours, inclusions were not completely re-homogenized. After the second one, conducted at 850 °C and 10 kbar for 24 hours, inclusions were almost completely remelted but they often showed interactions with the host garnets (they are overheated inclusions), indicating that the trapping temperature was exceeded. One inclusion was almost totally re-homogenized, without clear evidence of overheating.

Despite these experimental and analytical difficulties, I obtained for the first time, the probable composition of the melt produced by the partial melting of crustal rocks of the Valpelline Series. This melt shows a granitic composition ($SiO_2 \approx 72\%$, $Na_2O \approx 2\%$, $CaO \approx 0.7\%$, $K_2O \approx 6\%$, $FeO \approx 4\%$, $Al_2O_3 \approx 13\ \%$).

Because melt inclusions are partially remelted at 800 °C and often overheated at 850 °C, this work confirms the previous temperature estimates from the literature on peak conditions of the Variscan metamorphism. The presence of many nanogranites inclusions leaves the possibility of further analyses and studies in order to obtain (if it is possible) a more precise temperature of MI homogenization and to provide a more specific melt composition (e.g., trace elements).

Ringraziamenti

In primo luogo desidero ringraziare il Prof. Bernardo Cesare e il Dott. Omar Bartoli per i numerosi e preziosi insegnamenti che mi hanno dato e per la grande disponibilità e pazienza nel revisionare questo lavoro di tesi.

Per la parte sperimentale vorrei ringraziare il Dott. Luca Capizzi, Dipartimento di Scienze della Terra, Università di Milano, per avermi dato la possibilità di partecipare attivamente agli esperimenti fatti.

Ringrazio Leonardo Tauro, Dipartimento di Geoscienze, Università di Padova, per i consigli e l'aiuto datomi nelle fasi di preparazione dei campioni.

Un ultimo ringraziamento a Giorgio Vittorio dal Piaz, Bruno Monopoli, Prof. Michel Ballèvre, Geoscienze Renne, Università di Renne 1, e alla Prof.ssa Paola Manzotti, Dipartimento di Scienze della Terra (ISTE), Università di Losanna (UNIL), per le utili indicazioni e per la grande disponibilità datami durante il lavoro di campionamento.

References

Acosta-Vigil, A., Buick, I., Hermann, J., Cesare, B., Rubatto, D., London, D. and Morgan VI, G.B. (2010) Mechanisms of crustal anatexis: a geochemical study of partially melted metapelitic enclaves and host dacite, SE Spain. *Journal of Petrology* 51, 785–821.

Acosta-Vigil, A., Cesare, B., London, D. and Morgan VI, G.B. (2007) Microstructure and composition of melt inclusions in a crustal anatectic environment, represented by metapelitic enclaves within El Hoyazo Dacites, SE Spain. *Chemical Geology* 237, 450–65.

Bartoli, O., Cesare, B., Poli, S., Acosta-Vigil, A., Esposito, R., Turina, A., Bodnar, R.J., Angel R.J. and Hunter, J. (2013a) Nanogranite inclusions in migmatitic garnet: behavior during piston-cylinder remelting experiments. *Geofluids* 13, 405-420.

Bartoli, O., Cesare, B., Poli, S., Bodnar, R.J., Acosta-Vigil, A., Frezzotti, M.L. and Meli, S. (2013b) Recovering the composition of melt and the fluid regime at the onset of crustal anatexis and S-type granite formation. *Geology* 41, 115-118.

Bartoli, O., Cesare, B., Remusat, L., Acosta-Vigil, A. and Poli, S. (2014) The H_2O content of granite embryos. *Earth and Planetary Science Letters* 395, 281-290.

Bodnar, R.J. (2003) Reequilibration of fluid inclusions. In I. Samson, A. Anderson, & D. Marshall, eds. Fluid Inclusions: Analysis and Interpretation. *Mineral. Assoc. Canada, Short Course* 32, 213-230.

Brown, M. (1994) The generation, segregation, ascent and emplacement of granite magma: the migmatite-to-crustally-derived granite connection in thickened orogen. *Earth-Siences Reviews* 36, 83-130.

Carvalho, B., Bartoli, O., Ferri, F. and Cesare, B. (2018) Melt and fluid inclusions in metapelitic migmatites from Ivrea Zone: anatexis and fluid regime of a high-grade terrane. *Conference Paper.*

Cesare, B., Acosta-Vigil, A., Bartoli, O. and Ferrero, S. (2015) What can we learn from melt inclusions in migmatites and granulites?. *Lithos* 239, 186–216.

Cesare, B., Acosta-Vigil, A., Ferrero, S. and Bartoli, O. (2011) Melt inclusions in migmatites and granulites. *Journal of the Virtual Explorer* 38, paper 2.

Cesare, B., Ferrero, S., Salvioli-Mariani, E., Pedron, D. and Cavallo, A. (2009) "Nanogranite" and glassy inclusions: the anatectic melt in migmatites and granulites. *Geology* 37, 627–30.

Cesare, B., Maineri, C., Baron Toaldo, A., Pedron, D. and Cavallo, A. (2007) Immiscibility between carbonic fluids and granitic melts during crustal anatexis: a fluid and melt inclusion study in the enclaves of the Neogene Volcanic Province of SE Spain. *Chemical Geology* 237, 433-449.

Cesare, B., Salvioli-Mariani, E. and Venturelli, G. (1997) Crustal anatexis and melt extraction during deformation in the restitic xenoliths at El Joyazo (SE Spain). *Mineralogical Magazine* 61, 15–27.

Chupin, V.P., Kuzmin, D.V. and Madyukov, I.A. (2006) Melt inclusions in minerals of scapolite-bearing granulites (Lower crustal xenolites from diatremes of the Pamirs). *Doklady Earth Sciences* 407A, 507-511.

Compagnoni, R., Dal Piaz, G.V., Hunziker, J.C., Gosso, G., Lombardo, B. and Wlliams P.F. (1977b) The Sesia-Lonzo zone, a slice of continental crust with alpine high pressure-low temperature assemblages in the Western Italian Alps. *Rendiconti della Società Italiana di Mineralogia e Petrologia* 33, 281-334.

Dal Piaz, G.V. (1971). La II Zona Dioritico-Kinzigitica tra la Valsesia e la Valle d'Ayas (Alpi Ocidentali). *Memoria Delle Scienze Geologiche Italiane* 10, 257-278.

Dal Piaz, G.V. (1999) The Australpine-Piedmont nappe stack and the puzzle of Alpine Tethys. *Memorie Delle Scienze Geologiche Italiane* 51, 155-176.

Dal Piaz, G.V. (2001) Tertiary age and paleostructural inferences of the eclogitic imprint in the Australpine outliers and Zermatt-Sass ophiolite, Western Alps. *International Journal of Earth Sciences* 90, 668-684.

Dal Piaz, G.V., Bistacchi, A. and Massironi, M. (2003) Geological Outline of the Alps. *Episodes* 26, 175-180.

De Leo, S., Biino, G. and Compagnoni, R. (1987) Riequilibrazioni metamorfiche alpine della serie di Valpelline e di Arolla a nord di Bionaz (Valpelline-Aosta). *Rendiconti Della Societa Italiana Di Mineralogia e Petrologia* 42, 181.

Diehl, E.A., Masson, R. and Stutz, A.H. (1952) Contributo alla conoscenza del ricoprimento Dent Blanche. *Memorie degli Istituti di Geologia e Mineralogia dell'Università di Padova* 17, 5.

Ferrero, S., Bartoli, O., Cesare, B., Salvioli-Mariani, E., Acosta-Vigil, A., Cavallo, A., Groppo, C. and Battiston, S. (2012) Microstructures of melt inclusions in anatectic metasedimentary rocks. *Journal of Metamorphic Geology* 30, 303-22.

Ferrero, S., Wunder, B., Walczak, K., O'Brien, P.J. and Ziemann, M.A. (2015) Preserved near ultrahigh-pressure melt from continental crust subducted to mantle depths. *Geology* 43, 447-450.

Fossen, H. (2016) Structural Geology, Second Edition. *Cambridge University Press.*

Frezzotti, M.L. (2001) Silicate-Melt Inclusions in Magmatic Rocks: Applications to Petrology. *Lithos* 55, 273–99.

Gardien, V., Marquer, D. and Reusser, E. (1994) Pre-Alpine metamorphic evolution of the gneisses from the Valpelline serie (Western Alps, Italy). *Swiss Journal of Geosciences* 74, 489-502.

Goldstein, R.H. (2003) Petrographic analysis of fluid inclusions. *Fluid Inclusions-Analysis and Interpretation* 32, 9-54.

Handy, M.R., Schmid, S.M., Bousquet, R., Kissling, E. and Bernoulli, D. (2010) Reconciling plate-tectonic reconstructions of Alpine Tethys with the geological-geophysical record of spreading and subduction in the Alps. *Earth-Science Reviews* 102, 121–58.

Kohn, M.J. and Spear, F. (2000) Retrograde net transfer reaction insurance for pressure-temperature estimates. *Geology* 28, 1127-1130.

Kretz, R. (1983) Symbols for rock-forming minerals. *American Mineralogist* 68, 277-279.

Le Bayon, B. and Ballèvre, M. (2006) Deformation history of a subducted continental crust (Gran Paradiso, Western Alps): Continuing crustal shortening during exhumation. *Journal of Structural Geology* 28, 793-815.

Lowenstern, J.B. (1995) Applications of silicate-melt inclusions to the study of magmatic volatiles. *Mineralogical Association of Canada Short Course* 23, 71–99.

Manzotti, P. (2011) Petro-structural map of the Dent Blanche Tectonic System between Valpelline and Valtournenche Valleys,Western Italian Alps. *Journal of Maps* 7, 340-352.

Manzotti, P. and Zucali, M. (2013) The Pre-Alpine tectonic history of the Austroalpine continental basement in the Valpelline Unit (Western Italian Alps). *Geological Magazine* 150, 153-172.

Manzotti, P., Ballèvre, M., Zucali, M., Robyr, M. and Engi, M. (2014) The Tectonometamorphic Evolution of the Sesia–Dent Blanche Nappes (Internal Western Alps): Review and Synthesis. *Swiss Journal of Geosciences* 107, 309-336.

Manzotti, P., Rubatto, D., Darling, J., Zucali, M., Cenki-Tok, B. and Engi, M. (2012) From Permo-Triassic lithospheric thinning to Jurassic rifting at the Adriatic margin: petrological and geochronological record in Valtournenche (Western Italian Alps). *Lithos* 146–147, 276–92.

Marchildon, N. and Brown, M. (2001) Melt segregation in late syn-tectonic anatectic migmatites: an example from the Onawa contact aureole, Maine, USA. *Physics and Chemistry of the Earth*, Part A: Solid Earth and Geodesy 26, 225-229.

Maze, W.B., Bergman, S.C. and Sisson, V.B. (1981) Direct observations of the formation of fluid primary inclusions. *Geological Society of America* 13, 506.

Pennacchioni, G. and Guermani, A. (1993) The mylonites of the Australpine Dent Blanche nappe along the northwestern side of the Valpelline Valley (Italian Western Alps). *Memorie Scienze Geologiche* 45, 37-55.

Roedder, E. (1984) Fluid inclusions. *Mineralogical Society of America*, Reviews in Mineralogy 12, Mineralogical Society of America, Chantilly, Virginia.

Sawyer, E.W. (2008) Atlas of Migmatites. *Mineralogical Association of Canada. The Canadian Mineralogist, Special Publication* 9, Quebec City.

Sawyer, E.W. (2008) Identifying the parts of migmatites in the field in Working of Migmatites. *Mineralogical Association of Canada Short Course* 38, 29-36.

Sawyer, E.W. (2008) Working with migmatites: nomenclature for the consituent parts in Working with Migmatites. *Mineralogical Association of Canada Short* Course 38, 29-36.

Sisson, V.B., Lovelace, R.B., Maze, W.B. and Bergam, S.C. (1993) Direct observation of primary fluid inclusion formation. *Geology* 21, 751-754.

Touret, J.L.R. (2001) Fluids in Metamorphic Rocks. *Lithos* 55, 1-25.

Zucali, M. and Roda, M. (2008). Meso and microstructural evolution of the Mont Morion metaintrusive complex (Dent Blanche Nappe, Austroalpine Domain, Valpelline, Western Italian Alpas). *Italian Journal of Geosciences* 127, 105-123.

Zucali, M., and Spalla, M.I. (2011) Prograde lawsonite during the flow of continental crust in the Alpine subduction: strain vs. metamorphism partitioning, a filed-analysis approach to infer tectonometamorphic evolution (Sesia-Lanzo Zone, Western Italian Alps). *Journal of the Virtual Explorer* 33, 381-398.

Appendix

tab. 2. EMP analyses of the garnet from sample Valp11.

	Valp11-Rim1	Valp11-Rim2	Valp11-Rim3	Valp11-Rim4	Valp11-Rim5	Valp11-Rim6	Valp11-Rim7	Valp11-Rim8	Valp11-Rim9	Valp11-Rim10	Valp11-Rim11	Valp11-Rim12	Valp11-Rim13	Valp11-Rim14	Valp11-Rim15
MgO	7,60	8,01	7,62	7,62	7,54	8,41	7,85	7,62	7,73	7,80	7,71	7,66	7,61	7,61	7,65
Al_2O_3	21,72	21,88	21,80	22,07	21,88	21,86	22,00	22,09	21,76	22,16	22,00	21,88	21,82	22,06	21,88
SiO_2	38,58	37,61	38,08	38,48	38,14	37,69	38,42	38,42	38,30	38,54	38,27	38,47	38,55	38,30	38,35
CaO	3,68	3,36	3,55	3,56	3,56	3,50	3,48	3,50	3,44	3,51	3,57	3,48	3,57	3,54	3,46
TiO_2	0,00	0,06	0,05	0,02	0,04	0,03	0,03	0,03	0,03	0,04	0,05	0,04	0,05	0,04	0,04
MnO	1,29	1,22	1,21	1,19	1,30	1,19	1,16	1,18	1,24	1,33	1,27	1,28	1,26	1,24	1,22
FeO	28,40	28,38	28,50	28,29	28,32	28,44	28,52	28,19	28,79	28,56	28,63	28,47	28,41	28,48	28,45
Totale	**101,27**	**100,53**	**100,82**	**101,22**	**100,78**	**101,13**	**101,45**	**101,04**	**101,30**	**101,95**	**101,50**	**101,29**	**101,26**	**101,28**	**101,03**
Si	2,97	2,92	2,95	2,96	2,96	2,91	2,95	2,96	2,96	2,95	2,95	2,96	2,97	2,95	2,96
Ti	0,00	0,00	0,00	0,00	0,00	0,00	0,00	0,00	0,00	0,00	0,00	0,00	0,00	0,00	0,00
Al	1,97	2,01	1,99	2,00	2,00	1,99	1,99	2,01	1,98	2,00	2,00	1,99	1,98	2,00	1,99
Fe^{2+}	1,83	1,85	1,85	1,82	1,84	1,84	1,83	1,82	1,86	1,83	1,84	1,83	1,83	1,84	1,84
Mn	0,08	0,08	0,08	0,08	0,09	0,08	0,08	0,08	0,08	0,09	0,08	0,08	0,08	0,08	0,08
Mg	0,87	0,93	0,88	0,88	0,87	0,97	0,90	0,88	0,89	0,89	0,89	0,88	0,87	0,87	0,88
Ca	0,30	0,28	0,29	0,29	0,30	0,29	0,29	0,29	0,28	0,29	0,29	0,29	0,29	0,29	0,29
X_{prp}	0,28	0,30	0,28	0,29	0,28	0,31	0,29	0,29	0,29	0,29	0,29	0,29	0,28	0,28	0,29
X_{alm}	0,59	0,59	0,60	0,59	0,59	0,58	0,59	0,59	0,60	0,59	0,59	0,59	0,59	0,60	0,60
X_{sps}	0,03	0,03	0,03	0,03	0,03	0,02	0,02	0,03	0,03	0,03	0,03	0,03	0,03	0,03	0,03
X_{grs}	0,10	0,09	0,10	0,10	0,10	0,09	0,09	0,09	0,09	0,09	0,09	0,09	0,10	0,09	0,09

	Valp11-Rim16	Valp11-Rim17	Valp11-Rim18	Valp11-Rim19	Valp11-Rim20	Valp11-Rim21	Valp11-Rim22	Valp11-Rim23	Valp11-Rim24	Valp11-Rim25	Valp11-Rim26	Valp11-Rim27	Valp11-Rim28	Valp11-Rim29	Valp11Rim31
MgO	7,51	7,57	7,53	7,57	7,52	7,59	7,47	7,64	7,69	7,69	7,64	7,77	7,62	7,53	7,72
Al_2O_3	21,79	22,00	21,85	22,00	22,01	22,08	21,95	21,68	21,81	21,64	21,76	21,71	21,81	22,07	21,95
SiO_2	38,63	38,51	38,76	38,63	38,32	38,33	38,24	38,50	38,55	38,47	38,41	38,54	38,34	38,57	38,29
CaO	3,47	3,51	3,53	3,47	3,41	3,53	3,41	3,44	3,51	3,48	3,53	3,60	3,48	3,55	3,54
TiO_2	0,01	0,06	0,04	0,03	0,07	0,06	0,06	0,05	0,07	0,06	0,05	0,05	0,06	0,05	0,07
MnO	1,22	1,28	1,21	1,26	1,22	1,22	1,28	1,20	1,29	1,21	1,31	1,34	1,22	1,19	1,26
FeO	28,53	28,45	28,51	28,92	28,83	28,44	28,08	28,24	28,30	28,47	28,16	28,77	28,60	28,92	28,67
Totale	**101,14**	**101,38**	**101,43**	**101,88**	**101,37**	**101,26**	**100,49**	**100,75**	**101,23**	**101,02**	**100,86**	**101,78**	**101,12**	**101,88**	**101,50**
Si	2,98	2,96	2,98	2,96	2,95	2,95	2,97	2,98	2,97	2,97	2,97	2,96	2,96	2,96	2,95
Ti	0,00	0,00	0,00	0,00	0,00	0,00	0,00	0,00	0,00	0,00	0,00	0,00	0,00	0,00	0,00
Al	1,98	2,00	1,98	1,99	2,00	2,01	2,01	1,98	1,98	1,97	1,98	1,97	1,99	1,99	1,99
Fe^{2+}	1,84	1,83	1,83	1,86	1,86	1,83	1,82	1,83	1,82	1,84	1,82	1,85	1,85	1,86	1,85
Mn	0,08	0,08	0,08	0,08	0,08	0,08	0,08	0,08	0,08	0,08	0,09	0,09	0,08	0,08	0,08
Mg	0,86	0,87	0,86	0,87	0,86	0,87	0,86	0,88	0,88	0,89	0,88	0,89	0,88	0,86	0,89
Ca	0,29	0,29	0,29	0,29	0,28	0,29	0,28	0,29	0,29	0,29	0,29	0,30	0,29	0,29	0,29
X_{prp}	0,28	0,28	0,28	0,28	0,28	0,28	0,28	0,29	0,29	0,29	0,29	0,29	0,28	0,28	0,29
X_{alm}	0,60	0,60	0,60	0,60	0,60	0,60	0,60	0,59	0,59	0,59	0,59	0,59	0,60	0,60	0,59
X_{sps}	0,03	0,03	0,03	0,03	0,03	0,03	0,03	0,03	0,03	0,03	0,03	0,03	0,03	0,02	0,03
X_{grs}	0,09	0,09	0,09	0,09	0,09	0,09	0,09	0,09	0,09	0,09	0,09	0,10	0,09	0,09	0,09

	Valp11-Rim16	Valp11-Rim17	Valp11-Rim18	Valp11-Rim19	Valp11-Rim20	Valp11-Rim21	Valp11-Rim22	Valp11-Rim23	Valp11-Rim24	Valp11-Rim25	Valp11-Rim26	Valp11-Rim27	Valp11-Rim28	Valp11-Rim29	Valp11Rim31
MgO	7,51	7,57	7,53	7,57	7,52	7,59	7,47	7,64	7,69	7,69	7,64	7,77	7,62	7,53	7,72
Al_2O_3	21,79	22,00	21,85	22,00	22,01	22,08	21,95	21,68	21,81	21,64	21,76	21,71	21,81	22,07	21,95
SiO_2	38,63	38,51	38,76	38,63	38,32	38,33	38,24	38,50	38,55	38,47	38,41	38,54	38,34	38,57	38,29
CaO	3,47	3,51	3,53	3,47	3,41	3,53	3,41	3,44	3,51	3,48	3,53	3,60	3,48	3,55	3,54
TiO_2	0,01	0,06	0,04	0,03	0,07	0,06	0,06	0,05	0,07	0,06	0,05	0,05	0,06	0,05	0,07
MnO	1,22	1,28	1,21	1,26	1,22	1,22	1,28	1,20	1,29	1,21	1,31	1,34	1,22	1,19	1,26
FeO	28,53	28,45	28,51	28,92	28,83	28,44	28,08	28,24	28,30	28,47	28,16	28,77	28,60	28,92	28,67
Totale	**101,14**	**101,38**	**101,43**	**101,88**	**101,37**	**101,26**	**100,49**	**100,75**	**101,23**	**101,02**	**100,86**	**101,78**	**101,12**	**101,88**	**101,50**
Si	2,98	2,96	2,98	2,96	2,95	2,95	2,97	2,98	2,97	2,97	2,97	2,96	2,96	2,96	2,95
Ti	0,00	0,00	0,00	0,00	0,00	0,00	0,00	0,00	0,00	0,00	0,00	0,00	0,00	0,00	0,00
Al	1,98	2,00	1,98	1,99	2,00	2,01	2,01	1,98	1,98	1,97	1,98	1,97	1,99	1,99	1,99
Fe^{2+}	1,84	1,83	1,83	1,86	1,86	1,83	1,82	1,83	1,82	1,84	1,82	1,85	1,85	1,86	1,85
Mn	0,08	0,08	0,08	0,08	0,08	0,08	0,08	0,08	0,08	0,08	0,09	0,09	0,08	0,08	0,08
Mg	0,86	0,87	0,86	0,87	0,86	0,87	0,86	0,88	0,88	0,89	0,88	0,89	0,88	0,86	0,89
Ca	0,29	0,29	0,29	0,29	0,28	0,29	0,28	0,29	0,29	0,29	0,29	0,30	0,29	0,29	0,29
X_{prp}	0,28	0,28	0,28	0,28	0,28	0,28	0,28	0,29	0,29	0,29	0,29	0,29	0,28	0,28	0,29
X_{alm}	0,60	0,60	0,60	0,60	0,60	0,60	0,60	0,59	0,59	0,59	0,59	0,59	0,60	0,60	0,59
X_{sps}	0,03	0,03	0,03	0,03	0,03	0,03	0,03	0,03	0,03	0,03	0,03	0,03	0,03	0,02	0,03
X_{grs}	0,09	0,09	0,09	0,09	0,09	0,09	0,09	0,09	0,09	0,09	0,09	0,10	0,09	0,09	0,09

	Valp11-Rim32	Valp11-Rim33	Valp11-Rim34	Valp11-rim-35_1	Valp11-rim-35_2	Valp11-rim-35_3	Valp11-rim-35_4	Valp11-rim-35_5	Valp11-rim-35_6	Valp11-rim-35_7	Valp11-rim-35_8	Valp11-rim-35_9	Valp11-rim-35_10	Valp11-rim-35_11	Valp11-rim-35_12
MgO	7,67	7,50	7,64	7,57	7,76	7,56	7,58	7,59	7,61	7,69	7,78	7,54	7,68	7,73	7,70
Al_2O_3	21,97	21,66	21,90	21,88	21,82	21,77	21,78	21,82	21,89	21,89	21,70	22,05	21,74	21,68	21,61
SiO_2	38,41	38,22	38,46	38,33	38,48	38,63	38,37	38,53	38,46	38,50	38,54	38,51	38,44	38,53	38,40
CaO	3,59	3,48	3,53	3,50	3,55	3,51	3,47	3,46	3,43	3,42	3,46	3,50	3,56	3,38	3,43
TiO_2	0,04	0,07	0,05	0,06	0,04	0,06	0,08	0,07	0,08	0,07	0,06	0,09	0,05	0,05	0,07
MnO	1,32	1,20	1,23	1,30	1,25	1,12	1,24	1,28	1,26	1,24	1,21	1,20	1,23	1,12	1,29
FeO	28,41	28,18	28,63	28,53	28,46	28,45	28,57	28,53	28,36	28,42	28,59	28,67	28,52	28,45	28,47
Totale	**101,40**	**100,31**	**101,44**	**101,17**	**101,37**	**101,10**	**101,10**	**101,26**	**101,09**	**101,23**	**101,34**	**101,56**	**101,22**	**100,93**	**100,97**
Si	2,96	2,97	2,96	2,96	2,96	2,98	2,96	2,97	2,97	2,97	2,97	2,96	2,97	2,98	2,97
Ti	0,00	0,00	0,00	0,00	0,00	0,00	0,00	0,00	0,00	0,00	0,00	0,01	0,00	0,00	0,00
Al	1,99	1,99	1,99	1,99	1,98	1,98	1,98	1,98	1,99	1,99	1,97	2,00	1,98	1,97	1,97
Fe^{2+}	1,83	1,83	1,84	1,84	1,83	1,83	1,85	1,84	1,83	1,83	1,84	1,84	1,84	1,84	1,84
Mn	0,09	0,08	0,08	0,09	0,08	0,07	0,08	0,08	0,08	0,08	0,08	0,08	0,08	0,07	0,08
Mg	0,88	0,87	0,88	0,87	0,89	0,87	0,87	0,87	0,88	0,88	0,89	0,86	0,88	0,89	0,89
Ca	0,30	0,29	0,29	0,29	0,29	0,29	0,29	0,29	0,28	0,28	0,29	0,29	0,29	0,28	0,28
X_{prp}	0,28	0,28	0,28	0,28	0,29	0,28	0,28	0,28	0,29	0,29	0,29	0,28	0,29	0,29	0,29
X_{alm}	0,59	0,60	0,60	0,60	0,59	0,60	0,60	0,60	0,60	0,60	0,59	0,60	0,59	0,60	0,59
X_{sps}	0,03	0,03	0,03	0,03	0,03	0,02	0,03	0,03	0,03	0,03	0,03	0,03	0,03	0,02	0,03
X_{grs}	0,10	0,09	0,09	0,09	0,09	0,09	0,09	0,09	0,09	0,09	0,09	0,09	0,09	0,09	0,09

	Valp11-rim-35_13	Valp11-rim-35_14	Valp11-rim-35_15	Valp11-rim-35_16	Valp11-rim-35_17	Valp11-rim-35_18	Valp11-rim-35_19	Valp11-rim-35_20	Valp11-rim-35_21	Valp11-rim-35_22	Valp11-rim-35_23	Valp11-rim-35_24	Valp11-rim-35_25	Valp11-rim-35_26	Valp11-rim-35_27
MgO	7,54	7,64	7,71	7,62	7,56	7,57	7,64	7,55	7,44	7,54	7,65	7,57	7,64	7,54	7,67
Al_2O_3	22,11	21,76	21,88	21,96	21,96	22,01	21,87	22,13	21,94	21,83	21,75	22,02	21,87	22,08	21,78
SiO_2	38,22	38,38	38,15	38,05	38,56	38,23	38,48	38,47	38,31	38,33	38,75	38,44	38,32	38,18	38,46
CaO	3,52	3,48	3,46	3,46	3,42	3,39	3,39	3,53	3,40	3,41	3,40	3,47	3,41	3,36	3,46
TiO_2	0,01	0,06	0,07	0,06	0,02	0,04	0,04	0,02	0,04	0,04	0,03	0,04	0,08	0,04	0,04
MnO	1,17	1,17	1,25	1,18	1,31	1,23	1,30	1,25	1,08	1,18	1,29	1,19	1,11	1,23	1,22
FeO	28,64	28,61	28,76	28,64	28,73	28,50	28,25	28,54	28,53	28,83	28,54	28,89	28,45	28,64	28,44
Totale	**101,22**	**101,10**	**101,29**	**100,96**	**101,56**	**100,99**	**100,96**	**101,49**	**100,73**	**101,16**	**101,42**	**101,63**	**100,89**	**101,07**	**101,06**
Si	2,95	2,96	2,95	2,95	2,97	2,95	2,97	2,96	2,97	2,96	2,98	2,96	2,96	2,95	2,97
Ti	0,00	0,00	0,00	0,00	0,00	0,00	0,00	0,00	0,00	0,00	0,00	0,00	0,00	0,00	0,00
Al	2,01	1,98	1,99	2,00	1,99	2,01	1,99	2,01	2,00	1,99	1,97	2,00	1,99	2,01	1,98
Fe^{2+}	1,85	1,85	1,86	1,85	1,85	1,84	1,82	1,84	1,85	1,86	1,84	1,86	1,84	1,85	1,84
Mn	0,08	0,08	0,08	0,08	0,09	0,08	0,08	0,08	0,07	0,08	0,08	0,08	0,07	0,08	0,08
Mg	0,87	0,88	0,89	0,88	0,87	0,87	0,88	0,86	0,86	0,87	0,88	0,87	0,88	0,87	0,88
Ca	0,29	0,29	0,29	0,29	0,28	0,28	0,28	0,29	0,28	0,28	0,28	0,29	0,28	0,28	0,29
X_{prp}	0,28	0,28	0,29	0,28	0,28	0,28	0,29	0,28	0,28	0,28	0,29	0,28	0,29	0,28	0,29
X_{alm}	0,60	0,60	0,60	0,60	0,60	0,60	0,59	0,60	0,60	0,60	0,60	0,60	0,60	0,60	0,60
X_{sps}	0,02	0,02	0,03	0,02	0,03	0,03	0,03	0,03	0,02	0,03	0,03	0,03	0,02	0,03	0,03
X_{grs}	0,09	0,09	0,09	0,09	0,09	0,09	0,09	0,09	0,09	0,09	0,09	0,09	0,09	0,09	0,09

	Valp11-rim-35_28	Valp11-rim-35_29	Valp11-rim-35_30	Valp11-rim-35_31	Valp11-rim-35_32	Valp11-rim-35_33	Valp11-rim-35_34	Valp11-rim-35_35	Valp11-rim-35_36	Valp11-rim-35_37	Valp11-rim-35_38	Valp11-rim-35_39	Valp11-rim-35_40	Valp11-rim-35_41	Valp11-rim-35_42
MgO	7,51	7,64	7,62	7,67	7,64	7,68	7,66	7,56	7,60	7,53	7,50	7,56	7,55	7,48	7,61
Al_2O_3	21,82	21,89	21,77	21,78	21,76	21,95	21,93	21,71	21,85	21,95	21,93	21,97	21,82	22,00	21,93
SiO_2	38,48	38,21	38,13	38,38	38,38	38,43	38,33	38,21	38,31	38,18	38,29	38,40	38,41	38,20	38,47
CaO	3,36	3,44	3,48	3,51	3,37	3,40	3,45	3,39	3,44	3,39	3,32	3,41	3,39	3,48	3,51
TiO_2	0,05	0,08	0,05	0,01	0,06	0,01	0,05	0,03	0,02	0,02	0,03	0,02	0,01	0,00	0,00
MnO	1,26	1,22	1,24	1,19	1,29	1,27	1,20	1,26	1,13	1,28	1,25	1,22	1,20	1,36	1,30
FeO	28,68	29,14	28,69	28,66	28,90	28,62	28,78	28,62	28,39	28,66	28,57	28,88	28,50	28,54	28,74
Totale	**101,16**	**101,62**	**100,98**	**101,20**	**101,39**	**101,37**	**101,40**	**100,78**	**100,74**	**101,00**	**100,89**	**101,45**	**100,88**	**101,06**	**101,57**
Si	2,97	2,94	2,95	2,96	2,96	2,96	2,95	2,96	2,97	2,95	2,96	2,96	2,97	2,95	2,96
Ti	0,00	0,00	0,00	0,00	0,00	0,00	0,00	0,00	0,00	0,00	0,00	0,00	0,00	0,00	0,00
Al	1,99	1,99	1,99	1,98	1,98	1,99	1,99	1,98	1,99	2,00	2,00	1,99	1,99	2,00	1,99
Fe^{2+}	1,85	1,88	1,86	1,85	1,86	1,84	1,85	1,86	1,84	1,85	1,85	1,86	1,84	1,85	1,85
Mn	0,08	0,08	0,08	0,08	0,08	0,08	0,08	0,08	0,07	0,08	0,08	0,08	0,08	0,09	0,08
Mg	0,86	0,88	0,88	0,88	0,88	0,88	0,88	0,87	0,88	0,87	0,87	0,87	0,87	0,86	0,87
Ca	0,28	0,28	0,29	0,29	0,28	0,28	0,29	0,28	0,29	0,28	0,28	0,28	0,28	0,29	0,29
X_{prp}	0,28	0,28	0,28	0,28	0,28	0,29	0,28	0,28	0,29	0,28	0,28	0,28	0,28	0,28	0,28
X_{alm}	0,60	0,60	0,60	0,60	0,60	0,60	0,60	0,60	0,60	0,60	0,60	0,60	0,60	0,60	0,60
X_{sps}	0,03	0,03	0,03	0,03	0,03	0,03	0,03	0,03	0,02	0,03	0,03	0,03	0,03	0,03	0,03
X_{grs}	0,09	0,09	0,09	0,09	0,09	0,09	0,09	0,09	0,09	0,09	0,09	0,09	0,09	0,09	0,09

	Valp11-rim-35_44	Valp11-rim-35_45	Valp11-rim-35_46	Valp11-rim-35_47	Valp11-rim-35_48	Valp11-rim-35_49	Valp11-rim-35_50	Valp11-rim-35_51	Valp11-rim-35_52	Valp11-rim-35_53	Valp11-rim-35_54	Valp11-rim-35_55	Valp11-rim-35_56	Valp11-rim-35_57	Valp11-rim-35_58
MgO	7,52	7,58	7,60	7,55	7,59	7,49	7,53	7,44	7,50	7,50	7,43	7,55	7,35	7,51	7,42
Al_2O_3	22,15	22,06	21,96	22,04	22,00	21,79	22,01	22,03	21,85	21,90	21,97	21,92	22,03	21,95	22,02
SiO_2	38,29	38,49	38,45	38,39	38,59	38,46	38,31	38,24	38,25	38,56	38,09	38,23	38,08	38,29	38,45
CaO	3,39	3,39	3,38	3,43	3,41	3,41	3,36	3,45	3,42	3,45	3,42	3,50	3,36	3,48	3,42
TiO_2	0,02	0,04	0,03	0,04	0,02	0,01	0,01	0,04	0,03	0,01	0,02	0,01	0,03	0,01	0,01
MnO	1,23	1,19	1,25	1,23	1,19	1,23	1,19	1,28	1,30	1,36	1,30	1,22	1,31	1,21	1,31
FeO	28,80	28,84	29,00	28,65	28,72	28,96	28,73	28,80	28,44	28,76	29,00	28,84	28,64	29,19	28,47
Totale	**101,39**	**101,59**	**101,68**	**101,32**	**101,53**	**101,34**	**101,15**	**101,28**	**100,80**	**101,53**	**101,23**	**101,27**	**100,80**	**101,63**	**101,09**
Si	2,95	2,96	2,96	2,96	2,97	2,97	2,96	2,95	2,96	2,97	2,95	2,95	2,95	2,95	2,97
Ti	0,00	0,00	0,00	0,00	0,00	0,00	0,00	0,00	0,00	0,00	0,00	0,00	0,00	0,00	0,00
Al	2,01	2,00	1,99	2,00	1,99	1,98	2,00	2,00	2,00	1,99	2,00	2,00	2,01	1,99	2,00
Fe^{2+}	1,86	1,85	1,86	1,85	1,85	1,87	1,86	1,86	1,84	1,85	1,88	1,86	1,86	1,88	1,84
Mn	0,08	0,08	0,08	0,08	0,08	0,08	0,08	0,08	0,09	0,09	0,09	0,08	0,09	0,08	0,09
Mg	0,86	0,87	0,87	0,87	0,87	0,86	0,87	0,86	0,87	0,86	0,86	0,87	0,85	0,86	0,85
Ca	0,28	0,28	0,28	0,28	0,28	0,28	0,28	0,29	0,28	0,28	0,28	0,29	0,28	0,29	0,28
X_{prp}	0,28	0,28	0,28	0,28	0,28	0,28	0,28	0,28	0,28	0,28	0,28	0,28	0,28	0,28	0,28
X_{alm}	0,60	0,60	0,60	0,60	0,60	0,60	0,60	0,60	0,60	0,60	0,60	0,60	0,60	0,60	0,60
X_{sps}	0,03	0,03	0,03	0,03	0,03	0,03	0,03	0,03	0,03	0,03	0,03	0,03	0,03	0,03	0,03
X_{grs}	0,09	0,09	0,09	0,09	0,09	0,09	0,09	0,09	0,09	0,09	0,09	0,09	0,09	0,09	0,09

	Valp11-rim-35_59	Valp11-rim-35_60	Valp11-rim-35_61	Valp11-rim-35_62	Valp11-rim-35_63	Valp11-rim-35_64	Valp11-rim-35_65	Valp11-rim-35_66	Valp11-rim-35_67	Valp11-rim-35_68	Valp11-rim-35_69	Valp11-rim-35_70	Valp11-rim-35_71	Valp11-rim-35_72	Valp11-rim-35_73
MgO	7,49	7,52	7,49	7,51	7,40	7,39	7,37	7,38	7,36	7,30	7,36	7,29	7,33	7,29	7,27
Al_2O_3	21,84	22,08	21,97	22,12	21,90	21,85	21,76	22,01	21,90	21,83	22,02	22,00	22,09	22,07	21,91
SiO_2	38,28	37,99	38,21	38,20	38,25	38,09	38,30	38,22	38,37	38,43	38,40	38,10	37,93	38,28	38,15
CaO	3,43	3,41	3,44	3,39	3,54	3,57	3,48	3,46	3,46	3,38	3,46	3,39	3,49	3,53	3,56
TiO_2	0,04	0,02	0,01	0,01	0,00	0,02	0,03	0,01	0,04	0,02	0,00	0,03	0,03	0,04	0,03
MnO	1,34	1,21	1,30	1,26	1,18	1,32	1,20	1,31	1,21	1,27	1,27	1,25	1,17	1,22	1,29
FeO	28,53	28,66	28,90	28,74	28,19	28,97	29,18	29,00	29,12	28,96	29,18	29,22	28,82	29,35	29,14
Totale	**100,96**	**100,90**	**101,31**	**101,24**	**100,45**	**101,21**	**101,32**	**101,39**	**101,46**	**101,19**	**101,70**	**101,27**	**100,85**	**101,77**	**101,35**
Si	2,96	2,94	2,95	2,95	2,97	2,95	2,96	2,95	2,96	2,97	2,96	2,95	2,94	2,95	2,95
Ti	0,00	0,00	0,00	0,00	0,00	0,00	0,00	0,00	0,00	0,00	0,00	0,00	0,00	0,00	0,00
Al	1,99	2,02	2,00	2,01	2,00	1,99	1,98	2,00	1,99	1,99	2,00	2,01	2,02	2,00	2,00
Fe^{2+}	1,85	1,86	1,87	1,86	1,83	1,88	1,89	1,87	1,88	1,87	1,88	1,89	1,87	1,89	1,88
Mn	0,09	0,08	0,09	0,08	0,08	0,09	0,08	0,09	0,08	0,08	0,08	0,08	0,08	0,08	0,08
Mg	0,86	0,87	0,86	0,86	0,86	0,85	0,85	0,85	0,85	0,84	0,84	0,84	0,85	0,84	0,84
Ca	0,28	0,28	0,28	0,28	0,29	0,30	0,29	0,29	0,29	0,28	0,29	0,28	0,29	0,29	0,29
X_{prp}	0,28	0,28	0,28	0,28	0,28	0,27	0,27	0,27	0,27	0,27	0,27	0,27	0,27	0,27	0,27
X_{alm}	0,60	0,60	0,60	0,60	0,60	0,60	0,61	0,61	0,61	0,61	0,61	0,61	0,61	0,61	0,61
X_{sps}	0,03	0,03	0,03	0,03	0,03	0,03	0,03	0,03	0,03	0,03	0,03	0,03	0,02	0,03	0,03
X_{grs}	0,09	0,09	0,09	0,09	0,10	0,10	0,09	0,09	0,09	0,09	0,09	0,09	0,09	0,09	0,09

	Valp11-rim-35_74	Valp11-rim-35_75	Valp11-rim-35_76	Valp11-rim-35_77	Valp11-rim-35_78	Valp11-rim-35_79	Valp11-rim-35_80	Valp11-rim-35_81	Valp11-rim-35_82	Valp11-rim-35_83	Valp11-rim-35_84	Valp11-rim-35_85
MgO	7,05	7,25	7,15	7,21	6,98	7,08	6,93	6,84	6,63	6,83	6,62	5,96
Al_2O_3	22,02	21,92	21,74	21,77	21,75	22,06	21,86	21,79	22,33	21,99	22,08	21,64
SiO_2	38,12	38,34	38,11	38,32	38,06	38,31	38,25	38,42	39,09	38,11	38,19	37,88
CaO	3,57	3,59	3,52	3,60	3,71	3,65	3,73	3,75	3,88	3,86	3,94	4,27
TiO_2	0,05	0,03	0,05	0,03	0,04	0,03	0,00	0,02	0,00	0,05	0,05	0,01
MnO	1,24	1,23	1,19	1,29	1,28	1,28	1,27	1,24	1,26	1,30	1,25	1,30
FeO	28,86	28,90	28,78	28,89	29,35	29,40	29,09	29,00	29,09	29,19	29,58	29,50
Totale	**100,91**	**101,26**	**100,53**	**101,11**	**101,18**	**101,83**	**101,13**	**101,07**	**102,27**	**101,33**	**101,71**	**100,57**
Si	2,96	2,96	2,97	2,97	2,95	2,95	2,96	2,98	2,99	2,95	2,95	2,97
Ti	0,00	0,00	0,00	0,00	0,00	0,00	0,00	0,00	0,00	0,00	0,00	0,00
Al	2,01	2,00	1,99	1,99	1,99	2,00	2,00	1,99	2,01	2,01	2,01	2,00
Fe^{2+}	1,87	1,87	1,87	1,87	1,90	1,89	1,89	1,88	1,86	1,89	1,91	1,93
Mn	0,08	0,08	0,08	0,08	0,08	0,08	0,08	0,08	0,08	0,08	0,08	0,09
Mg	0,81	0,83	0,83	0,83	0,81	0,81	0,80	0,79	0,75	0,79	0,76	0,70
Ca	0,30	0,30	0,29	0,30	0,31	0,30	0,31	0,31	0,32	0,32	0,33	0,36
X_{prp}	0,27	0,27	0,27	0,27	0,26	0,26	0,26	0,26	0,25	0,26	0,25	0,23
X_{alm}	0,61	0,61	0,61	0,61	0,61	0,61	0,61	0,61	0,62	0,61	0,62	0,63
X_{sps}	0,03	0,03	0,03	0,03	0,03	0,03	0,03	0,03	0,03	0,03	0,03	0,03
X_{grs}	0,10	0,10	0,10	0,10	0,10	0,10	0,10	0,10	0,11	0,10	0,11	0,12